Article

Agonists for cytosolic bacterial receptor ALPK1 induce antitumour immunity

https://doi.org/10.1038/s41586-025-09828-9

Received: 5 September 2024

Accepted: 29 October 2025

Published online: 10 December 2025

Check for updates

Xiaoying Tian[1,2,9], Jiaqi Liu[1,2,9], Yuxi Li[2], Yupeng Wang[2], Yuanhanyu Luo[2], Huabin He[2], Yang She[2], Yan Ma[2], Jingjin Ding[2,3], Ping Zhou[2,4], Chao Li[2] & Feng Shao[2,3,5,6,7,8]✉

Targeting innate immunity holds promise in cancer immunotherapy, particularly in improving checkpoint inhibitors. However, the use of agonists of the promising innate receptors TLRs and STING[1–4] is facing challenges. Here we examined the antitumour function of the α-kinase 1 (ALPK1) receptor for bacterial ADP-heptose (ADP-Hep)[5–7]. Treatment of mice with ADP-Hep induced multiple proinflammatory factors including CXCL10 and CCL2, and stimulated *Alpk1*-dependent antitumour immunity. Mice bearing a gain-of-function ALPK1(T237M) disease variant[8] also rejected grafted tumours. Using medicinal chemistry, we identified a more potent analogue, UDSP-Hep. In contrast to ADP-Hep, UDSP-Hep distinguished *Alpk1* polymorphism, which correlates with mouse susceptibility to bacteria-associated colitis[9–12]. UDSP-Hep exhibited a stronger *Alpk1*-mediated antitumour effect and synergized with checkpoint inhibitors. The effect required $CD8^+$ T cells, dendritic cells (DCs) and macrophages, and was sensitive to antibodies that block CXCL10 or CCL2 function. ALPK1 agonists activated DCs for cross-presentation, promoting tumour-specific T cell expansion in the tumour-draining lymph nodes. ALPK1 has wider expression than STING in non-immune cells with a distinct inflammatory signature. UDSP-Hep is differentiated from STING agonists in stimulating tumour-cell antigen presentation, macrophage–DC cross-priming and protective memory T cell differentiation, and it does not induce T cell apoptosis. Our study elucidates the antitumour effect of ALPK1 agonism and suggests the potential of ALPK1 agonists in cancer immunotherapy.

In cancer immunotherapy, blockade of the T cell activation checkpoint proteins PD-1 and CTLA-4 is effective in only a small fraction of patients. Research has been undertaken to better understand immune escape and clearance of tumours and to develop immunotherapy strategies. A widely agreed notion is that effective tumour immunity requires certain proinflammatory responses, probably by activating innate immunity[13,14]. Indeed, small-molecule agonists for classical innate receptors such as TLR7, TLR8 and TLR9 (TLR7/8/9) and STING are being actively pursued but have not succeeded in humans. Different from TLR7/8/9 and STING, which sense nuclear acids and activate interferon signalling, the ALPK1 receptor recognizes ADP-Hep and mainly induces NF-κB-targeted gene transcription by phosphorylating Thr9 of TIFA[5–7]. ADP-Hep is a precursor in bacterial lipopolysaccharide (LPS) biosynthesis and is also present in other kingdoms of life[15]. ALPK1 activation not only mediates host defences against various bacterial infections[5,7,16–18] but it also underlies intestinal immune homeostasis[19,20].

Alpk1 and *Tifa* are adjacently located on mouse chromosome 3 within the *Helicobacter hepaticus*-induced colitis and associated cancer susceptibility[9,10] and cytokine-deficiency-induced colitis susceptibility-1[11,12] locus (hereafter, the *Hiccs*/*Cdcs1* locus); *Alpk1* polymorphism determines the susceptibility of 129 mice but not C57BL/6 mice to innate-driven colitis[9]. Mutations in *ALPK1* cause retinal dystrophy, optic nerve oedema, splenomegaly, anhidrosis and headache (ROSAH) syndrome[8,21–24] or predispose to the periodic fever, aphthous stomatitis, pharyngitis and adenitis (PFAPA) syndrome[25]. The ROSAH mutant T237M results in a partial gain of function, causing NF-κB activation[21]. ADP-Hep can enter mammalian cells autonomously; injection of ADP-Hep into the mouse dorsal air pouches induces systemic inflammation[5]. Together, this prompted us to examine the immunological properties of ALPK1 ligand and antitumour immune functions of the ADP-Hep–ALPK1 axis.

ADP-Hep is an innate immune agonist

Furthering our previous study[5], extracellular addition of ADP-Hep to wild-type mouse bone-marrow-derived macrophages (BMDMs), but not *Alpk1*$^{-/-}$ BMDMs, stimulated NF-κB-targeted cytokine/chemokine transcription, including *Cxcl10*, *Ccl2*, *Il1b*, *Ccl4* and *Ccl9* (Extended Data Fig. 1a). ADP-Hep induced similar proinflammatory responses in human peripheral blood mononuclear cells (PBMCs) (Extended Data Fig. 1b). Intravenous injection of ADP-Hep into wild-type C57BL/6 mice

[1]Graduate School of Peking Union Medical College and Chinese Academy of Medical Sciences, Beijing, P. R. China. [2]National Institute of Biological Sciences, Beijing, P. R. China. [3]Key Laboratory of Biomacromolecules (CAS), National Laboratory of Biomacromolecules, CAS Center for Excellence in Biomacromolecules, Institute of Biophysics, Chinese Academy of Sciences, Beijing, P. R. China. [4]State Key Laboratory of Oncology in South China, Sun Yat-sen University Cancer Center, Guangdong Provincial Clinical Research Center for Cancer, Sun Yat-sen University, Guangzhou, P. R. China. [5]Research Unit of Pyroptosis and Immunity, Chinese Academy of Medical Sciences, Beijing, P. R. China. [6]Tsinghua Institute of Multidisciplinary Biomedical Research, Tsinghua University, Beijing, P. R. China. [7]Changping Laboratory, Beijing, P. R. China. [8]New Cornerstone Science Laboratory, Shenzhen, P. R. China. [9]These authors contributed equally: Xiaoying Tian, Jiaqi Liu. ✉e-mail: shaofeng@nibs.ac.cn

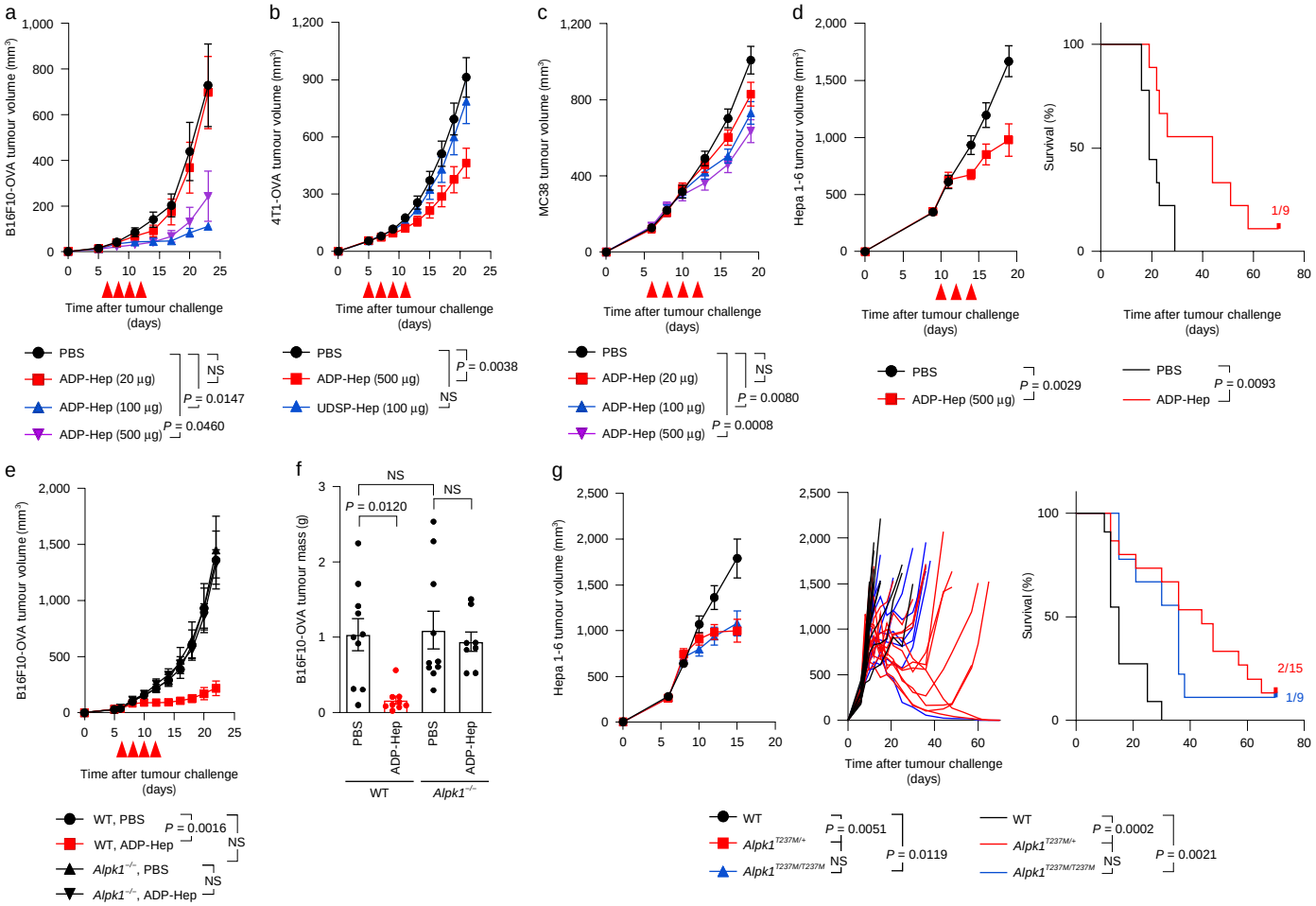

Fig. 1 | ALPK1 activation induces antitumour responses in mice. a,**c**,**d**, Growth curves (**a**,**c**,**d**) and mouse survival (**d**; fraction of surviving mice is shown) of B16F10-OVA melanoma (**a**), MC38 colon carcinoma (**c**) and Hepa 1-6 hepatoma (**d**) grafted subcutaneously into C57BL/6 mice. **b**, Growth curves of 4T1-OVA mammary carcinoma grafted subcutaneously into BALB/c mice. For **a**–**d**, the mice were treated with PBS or the indicated dose of ADP-Hep or UDSP-Hep ($n = 7$ (**a**), $n = 9$ for PBS and 8 for other groups (**b**); $n = 12$ for 500 μg ADP-Hep treatment and 11 for other groups (**c**); $n = 9$ per group (**d**)). **e**,**f**, wild-type (WT) or *Alpk1*$^{-/-}$ C57BL/6 mice bearing B16F10-OVA tumours were treated with PBS ($n = 10$) or ADP-Hep (500 μg per mouse, $n = 9$ for wild type and 8 for *Alpk1*$^{-/-}$). **e**, Tumour growth curves. **f**, The tumour weight on day 22 after tumour challenge. **g**, Hepa 1-6 tumours were grafted subcutaneously into wild-type ($n = 11$), *Alpk1*$^{T237M/+}$ ($n = 15$) or *Alpk1*$^{T237M/T237M}$ ($n = 9$) C57BL/6 mice. Left, average tumour growth curves. Middle, tumour growth curves in individual animals. Right, mouse survival; the fraction of surviving mice is shown. For **a**–**e** and **g**, the average tumour growth is shown for the period when all mice within the group remained on study. The red triangle indicates the post-tumour-grafting date when ADP-Hep/UDSP-Hep was injected. For **a**–**f** and **g**, data are mean ± s.e.m. Statistical analysis was performed using two-way analysis of variance (ANOVA) (**a**–**g**) and log-rank (Mantel–Cox) tests (**d** and **g**); NS, not significant. All data are representative of three independent experiments.

markedly elevated serum levels of CXCL10, CCL2, CCL3 (also known as MIP-1α), CCL4 (also known as MIP-1β), CCL5 (also known as RANTES), CCL7 (also known as MCP-3), CXCL1 (also known as GRO-α) and CXCL2 (also known as MIP-2) (Extended Data Fig. 1c). Such responses, resembling the inflammatory signature of patients with ROSAH[21], disappeared in *Alpk1*$^{-/-}$ and *Tifa*$^{-/-}$ mice (Extended Data Fig. 1c). ADP-Hep activated similar immune responses when injected into mice intraperitoneally, subcutaneously or intramuscularly (Extended Data Fig. 1d). Co-injection of ADP-Hep with ovalbumin (OVA) into C57BL/6 mice stimulated anti-OVA antibody production (Extended Data Fig. 1e), suggesting activation of adaptive immunity.

ADP-Hep induces antitumour responses

We next explored antitumour effect after ALPK1 activation. In the OVA-conjugated B16F10 (B16F10-OVA) subcutaneous melanoma model, intratumoural injections of ADP-Hep efficiently inhibited the tumour growth (Fig. 1a). ADP-Hep also controlled 4T1-OVA mammary carcinoma in BALB/c mice (Fig. 1b). Tumour inhibition was also noted in non-OVA-conjugated MC38 colon carcinoma and Hepa 1-6 hepatocellular carcinoma, even when the size of Hepa 1-6 tumours had reached around 500 mm^3 (Fig. 1c,d). The antitumour effect of ADP-Hep was diminished in *Alpk1*$^{-/-}$ mice (Fig. 1e,f and Extended Data Fig. 1f). Thus, ALPK1-mediated immune responses in host mice mainly drive the tumour control.

Alpk1^{T237M} knockin mice develop subclinical inflammation with elevated cytokine/chemokine production, particularly CXCL1, CXCL10 and CCL2, echoing the inflammatory signature in patients with ROSAH[21]. Notably, MC38 and Hepa 1-6 tumours grew more slowly in *Alpk1*$^{T237M/+}$ or *Alpk1*$^{T237M/T237M}$ mice compared with in their wild-type littermates (Fig. 1g and Extended Data Fig. 1g). This highlights an intrinsic antitumour function of the ADP-Hep–ALPK1 pathway.

UDSP-Hep is a more potent ALPK1 agonist

Given the potential of ALPK1 agonists in cancer immunotherapy, we synthesized a series of ADP-Hep analogues. First, the nucleoside of ADP-Hep was changed to cytidine, uridine, guanosine or their

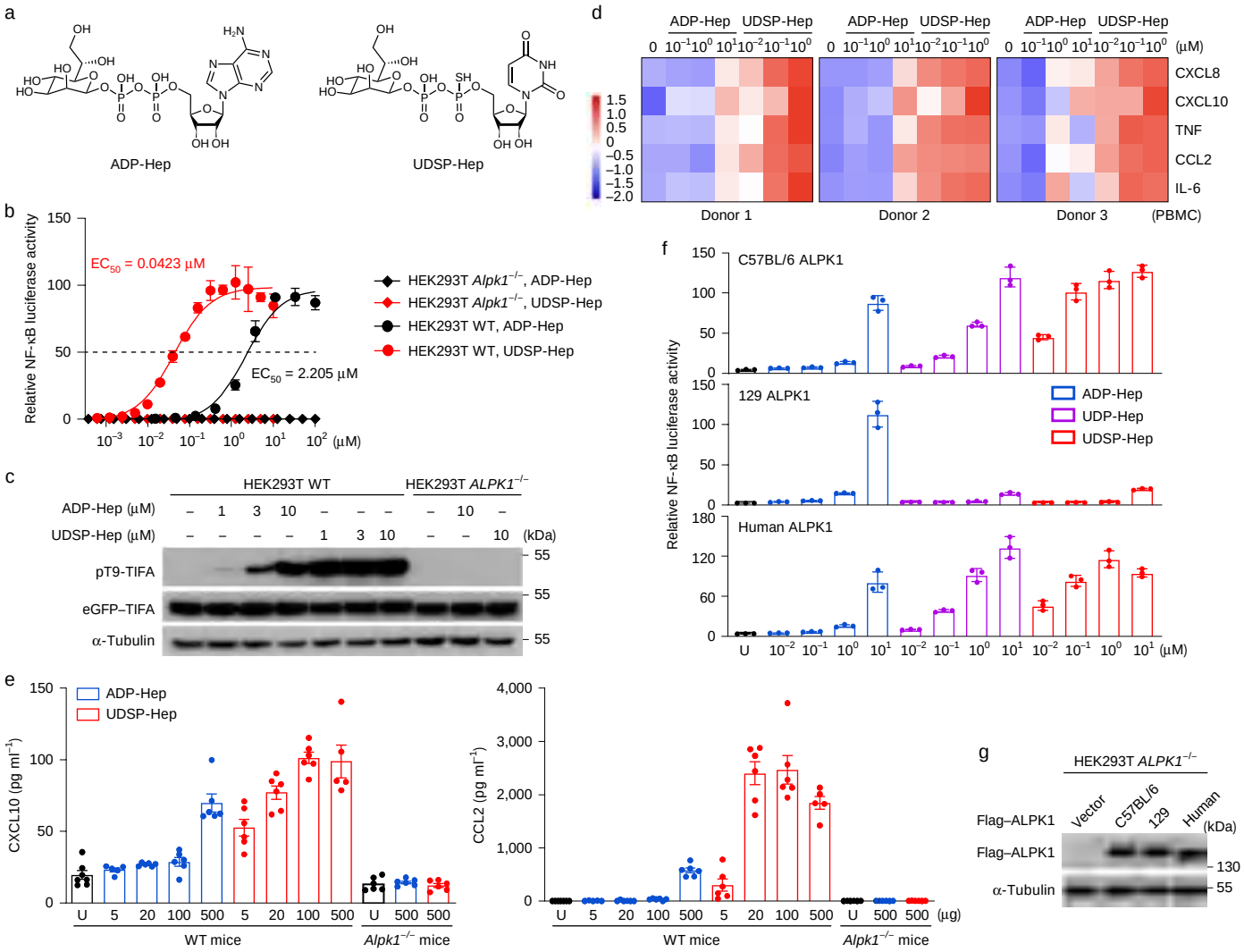

Fig. 2 | UDSP-Hep is a much more potent agonist and distinguishes polymorphic *Alpk1* alleles in mice. a, Chemical structures of ADP-Hep and UDSP-Hep. **b**, EC_{50} of ADP-Hep or UDSP-Hep in activating the NF-κB luciferase reporter. **c**, Wild-type or *ALPK1*$^{-/-}$ HEK293T cells with eGFP–TIFA integrated into the genome were treated as indicated. Anti-phosphorylated TIFA (Thr9) immunoblots (pT9-TIFA) are shown. **d**, Relative cytokine concentrations in the supernatants of ADP-Hep- or UDSP-Hep-treated human PBMCs (three donors), indicated by the colour scale. **e**, Wild-type or *Alpk1*$^{-/-}$ C57BL/6 mice were injected intravenously with ADP-Hep or UDSP-Hep. $n = 7$ (untreated (U) wild type), $n = 5$ (5 μg ADP-Hep- and 500 μg UDSP-Hep-treated wild type) and $n = 6$ (other groups). Representative cytokine concentrations in the sera are shown. Data are mean ± s.e.m. Statistical analysis was performed using two-way ANOVA. **f**,**g**, *ALPK1*$^{-/-}$ HEK293T cells expressing Flag–ALPK1 derived from C57BL/6 or 129 mice or humans were treated with the indicated agonist. **f**, NF-κB luciferase reporter activation. **g**, Anti-Flag immunoblotting. For **a** and **f**, data are mean ± s.d. $n = 3$. All data are representative of three independent experiments.

deoxy forms (Extended Data Fig. 2a and Supplementary Data 1). The half-maximum effective concentration (EC_{50}) of the derivatives was determined using the NF-κB reporter assay (Supplementary Fig. 1a). UDP-Hep and CDP-Hep showed around 20–40-fold increases in potency, while the activities of GDP-Hep and dTDP-Hep decreased by around 10–50-fold (Extended Data Fig. 2a). Consistently, UDP-Hep and CDP-Hep stimulated TIFA phosphorylation more robustly than ADP-Hep and other derivatives in HEK293T cells (Extended Data Fig. 2b). We also modified the ribose in adenosine (Extended Data Fig. 2a and Supplementary Data 1). Luciferase-reporter and TIFA-phosphorylation assays showed that ADP-OMe-Hep, ADP-F-Hep and ADP-deO-Hep were equally or slightly more active than ADP-Hep, while ADP-S-Hep had reduced activity (Extended Data Fig. 2a,b). We further synthesized phosphothioate versions of ADP-Hep and UDP-Hep to prevent non-specific hydrolysis and increase their serum stability (Extended Data Fig. 2a,c and Supplementary Data 1). ADSP-Hep and UDSP-Hep were much more potent in stimulating ALPK1 activation compared with ADP-Hep and UDP-Hep, respectively (Extended Data Fig. 2a,b). In contrast to in ADP-Hep, fluorine modification of the ribose in UDSP-Hep substantially reduced its activity. Among all of the analogues, UDSP-Hep was the most active, and its EC_{50} reached 0.0423 μM, around 50 times lower than that of ADP-Hep (Fig. 2a,b). UDSP-Hep was inactive in *ALPK1*-deficient cells (Fig. 2b,c). The substantially increased activity of UDSP-Hep was mainly due to its higher stability both in serum-containing medium and mammalian cell cytosol, and not due to an intrinsic ability to activate ALPK1 (Extended Data Fig. 2c–g).

In human PBMCs and THP-1 monocytes, UDSP-Hep induced proinflammatory cytokine/chemokine production to a much greater extent than ADP-Hep and UDP-Hep (Fig. 2d, Extended Data Fig. 3a and Supplementary Fig. 1b). Intravenous injection of UDSP-Hep into wild-type but not *Alpk1*$^{-/-}$ C57BL/6 mice also elicited higher levels of proinflammatory factors, including CXCL10, CCL2, CCL4, CCL7, CXCL1, CXCL2 and IL-6 (Fig. 2e and Extended Data Fig. 3b). Similar results were obtained after intraperitoneal, subcutaneous or intramuscular injection of UDSP-Hep (Supplementary Fig. 1c). UDSP-Hep promoted anti-OVA production in C57BL/6 mice in an *Alpk1*-dependent manner, also more prominently

than ADP-Hep (Extended Data Fig. 3c). Thus, UDSP-Hep is a highly potent ALPK1 agonist in human cells and mice.

UDSP-Hep discerns *Alpk1* alleles in mice

While assaying antitumour functions of UDSP-Hep, we found that UDSP-Hep, in contrast to ADP-Hep, could not control 4T1-OVA tumours in BALB/c mice (Fig. 1b). This contradicts the higher ALPK1-stimulating activity in UDSP-Hep, as seen in C57BL/6 mice (Extended Data Fig. 3d). We hypothesized that the mouse genetic background might affect the response to certain ALPK1 agonists. Indeed, UDSP-Hep, in contrast to ADP-Hep, induced minimal cytokine production in BALB/c and 129 mice (Extended Data Fig. 3d). UDSP-Hep did not induce anti-OVA production in BALB/c and 129 mice, despite its higher efficiency compared with ADP-Hep in C57BL/6 mice (Extended Data Fig. 3e). The unique strain-dependent activity in UDSP-Hep was similarly observed in BMDMs from different strains (Extended Data Fig. 3f). UDP-Hep behaved similarly to UDSP-Hep, suggesting that the uridine substitution of adenosine confers the mouse-stain selectivity of UDSP-Hep.

Previous analyses of the *Hiccs/Cdcs1* locus indicate that *Alpk1* in 129 mice is functionally attenuated, resulting in the susceptibility to bacteria-related, innate-driven colitis[9,10]. Indeed, *Alpk1* is polymorphic; the encoded ALPK1(BALB/c) and ALPK1(129) proteins are identical but have 17-residue differences compared with ALPK1(C57BL/6). When expressed in *ALPK1*$^{-/-}$ cells, ALPK1(C57BL/6), like human ALPK1, responded well to ADP-Hep and more robustly to UDP-Hep or UDSP-Hep, whereas ALPK1(129) responded only to ADP-Hep (Fig. 2f,g and Extended Data Fig. 3g). Thus, ALPK1(129) is greatly attenuated in sensing UDP-Hep, and UDP-Hep might be more relevant to the aetiology of *Hiccs/Cdcs1*-rendered colitis. This also suggests that C57BL/6 mice should be used for therapeutic developments of an ALPK1 agonist.

We tested the ability of UDSP-Hep to activate human ALPK1 variants, including the most frequent non-synonymous SNPs in *ALPK1*-coding region recorded in population datasets (gnomAD) and The Cancer Genome Atlas (TCGA). All of the tested variants responded robustly to UDSP-Hep, and the TIFA variants recorded in TCGA also showed no apparent differences compared to wild-type TIFA (Supplementary Fig. 2a–f).

UDSP-Hep has stronger antitumour effects

UDSP-Hep and C57BL/6-based syngeneic tumours were next used to investigate the antitumour functions of ALPK1 agonism. For this, we quantified the systemic bioavailability of subcutaneously administered UDSP-Hep, which was around 80% (Extended Data Fig. 3h). After peritumoural administration in mice, UDSP-Hep achieved appreciable concentrations in tumours (1.282 ± 0.49 μg per g) and tumour-draining lymph nodes (tdLNs) (0.471 ± 0.14 μg per g) (Extended Data Fig. 3i). UDSP-Hep, at a much lower dose than that required for ADP-Hep (Fig. 1a), caused nearly complete regression of B16F10-OVA, MC38 and Hepa1-6 tumours—an effect that was absent in *Alpk1*$^{-/-}$ mice (Fig. 3a and Extended Data Fig. 4a,b). UDSP-Hep treatment of as low as 30 μg per mouse nearly eliminated MB49 bladder carcinoma (Fig. 3a). Consistent with its equal potency on ALPK1(C57BL/6) and human ALPK1, UDSP-Hep efficiently restricted MC38 tumours in *ALPK1*-humanized mice (Fig. 3a). UDSP-Hep was inactive in immune-deficient NSG mice (Extended Data Fig. 4c,d) and did not affect cancer cell viability in vitro (Supplementary Fig. 2g). After a secondary tumour challenge in the Hepa1-6 model, mice whose initial tumours had been cleared by UDSP-Hep completely resisted the rechallenge (Fig. 3b). Thus, ALPK1 activation can induce an enduring antitumour immune memory in certain models. Moreover, when mice were grafted bilaterally with MC38 tumours, injection of UDSP-Hep into the right-side tumour caused comparable tumour inhibition at both sides (Fig. 3c). A similar distal effect was noted in Hepa1-6 and B16F10-OVA models (Extended Data Fig. 4e,f). Furthermore, UDSP-Hep and ADP-Hep evidently inhibited orthotopic E0771 and 4T1-OVA breast tumours, respectively (Extended Data Fig. 4g,h). Thus, agonizing ALPK1 with small molecules stimulates antitumour immunity in mice.

UDSP-Hep enhances checkpoint inhibitors

We examined whether ALPK1 activation could enhance the efficacy of immune checkpoint inhibitors (ICIs) or enable them to control resistant tumours. In the MC38 model, combining anti-CTLA-4 with UDSP-Hep led to markedly improved tumour control and prolonged mouse survival compared with infection of either agent alone (Fig. 3d and Extended Data Fig. 4i). Similar results were noted for the combination of anti-PD-1 and UDSP-Hep, after which nearly 70% of mice were cured (Fig. 3d and Extended Data Fig. 4j). High efficacy remained when the doses of UDSP-Hep and anti-PD-1 were lowered to levels such that either agent alone only had negligible effects (Extended Data Fig. 4j). Even for late-stage MC38 tumours (size of nearly 400 mm^3), more than half of the mice receiving UDSP-Hep and anti-PD-1 combination therapy exhibited sustained tumour regression for up to 60 days without recurrence (Extended Data Fig. 4k). UDSP-Hep could also work together with anti-4-1BB and anti-PD-L1 (Extended Data Fig. 4l,m). In native B16F10 tumours, UDSP-Hep, anti-CTLA-4 or anti-PD-1 alone showed little effects (Fig. 3e), but combining UDSP-Hep with either of the ICIs resulted in evident or substantial tumour control (Fig. 3e). These indicate a broad applicability of ALPK1 agonism in fostering antitumour immunity.

UDSP-Hep action requires CXCL10 and CCL2

Systemic administration of ALPK1 agonist into mice stimulated pro-inflammatory responses (Fig. 2e and Extended Data Fig. 3b). A single intratumoural injection of UDSP-Hep into B16F10-OVA tumours elevated levels of CCL2, CXCL10, CCL5 and TNF in the tumour interstitial fluid (TIF) (Fig. 4a). These cytokines and chemokines as well as IFNγ were similarly induced in the TIF of Hepa1-6 tumours (Extended Data Fig. 5a,b). Pertussis toxin (PTx) abrogated the antitumour effects of UDSP-Hep, indicating a requirement of chemokine receptor signalling (Extended Data Fig. 5c). Throughout our study, we consistently observed CXCL10 and CCL2 induction by ALPK1 agonists in cellular and mouse systems. The two chemokines also increased in *Alpk1*^{T237M} knockin mice[21]. CXCL10 and CCL2 have positive roles in antitumour immunity[26–30]. Administration of anti-CXCR3 (the receptor of CXCL10) or anti-CCL2 neutralizing antibodies reversed the restriction of MC38 and B16F10-OVA tumours by UDSP-Hep (Fig. 4b and Extended Data Fig. 5d). Thus, CXCL10 and CCL2 are essential for ALPK1-stimulated antitumour immunity.

Macrophages and monocytes responded robustly to ALPK1 agonism, secreting cytokines and chemokines including CCL2 and CXCL10. Depletion of macrophages using anti-CSF1R or clodronate liposomes diminished the antitumour effects of UDSP-Hep in the B16F10-OVA and Hepa1-6 models (Fig. 4c and Extended Data Fig. 5e). In a bone marrow chimera assay, UDSP-Hep could control B16F10-OVA tumours in chimeras with wild-type-to-wild-type haematopoiesis but not in the *Alpk1*$^{-/-}$-to-wild-type and wild-type-to-*Alpk1*$^{-/-}$ chimeras (Extended Data Fig. 5f). Thus, haematopoietic *Alpk1* is required but is not sufficient for ALPK1-mediated activation of antitumour immunity. Consistently, single-cell RNA-sequencing (scRNA-seq) analysis of B16F10-OVA tumours revealed high expression of ALPK1 and TIFA not only in myeloid cells but also in tumour cells within the tumour microenvironment (TME) (Extended Data Fig. 5g).

CD8$^+$ T cells mediate UDSP-Hep function

CCL2 and CXCL10 coordinate the recruitment of monocytes and lymphocytes, respectively[28,31]. Analyses of the TME in UDSP-Hep-treated

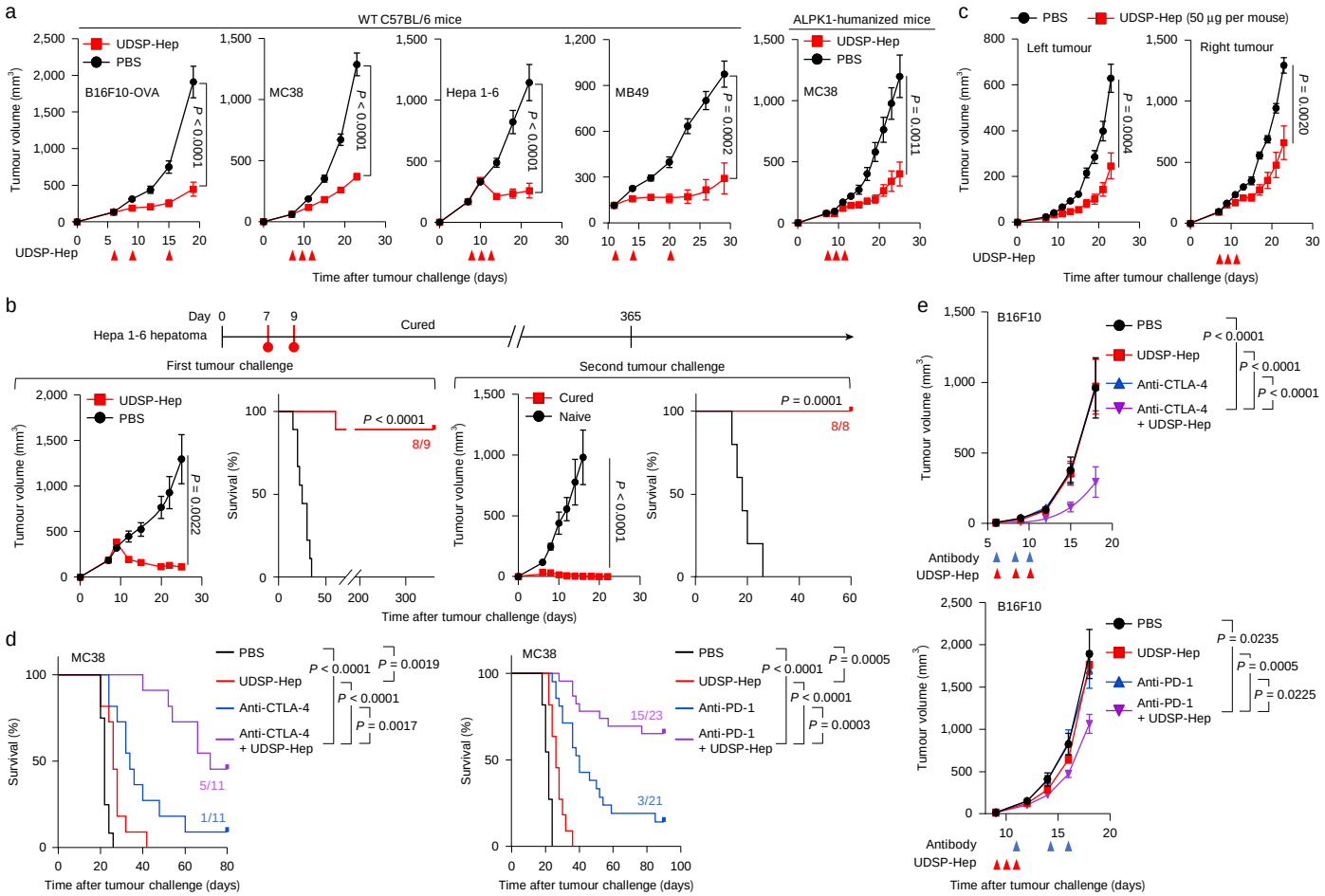

Fig. 3 | UDSP-Hep controls tumour growth alone or in combination with checkpoint inhibitors. a, Growth curves of B16F10-OVA melanoma, MC38 colon carcinoma, Hepa 1-6 hepatoma and MB49 bladder carcinoma in the indicated mice treated with PBS (left to right: $n = 11, 12, 15, 7$ and 11) or UDSP-Hep (left to right: 100 µg per mouse ($n = 10$), 50 µg per mouse ($n = 10$), 50 µg per mouse ($n = 17$), 30 µg per mouse ($n = 9$) and 50 µg per mouse ($n = 10$)). **b**, C57BL/6 mice bearing Hepa 1-6 tumours were treated with PBS or UDSP-Hep (50 µg per mouse). $n = 9$ mice per group. On day 365, mice with tumours cleared ($n = 8$) and additional naive mice ($n = 5$) were rechallenged with double doses of Hepa 1-6 cells. Tumour growth curves and mouse survival plots are shown. The fraction of surviving mice is shown. **c**, MC38 tumours were grafted into both sides of the back of C57BL/6 mice. PBS or UDSP-Hep were intratumourally injected into the right flank. $n = 8$ mice per group. **d**, Survival of MC38-tumour-bearing mice treated with PBS (left ($n = 12$), right ($n = 11$)), UDSP-Hep ($n = 11$; 50 µg per mouse), anti-CTLA-4 ($n = 11$; 0.5 mg per kg), anti-PD-1 ($n = 21$; 5 mg per kg), or UDSP-Hep1 combined with anti-CTLA-4 ($n = 11$) or anti-PD-1 ($n = 23$). The fraction of surviving mice is shown. **e**, Growth curves of B16F10 tumours in C57BL/6 mice treated with PBS (top ($n = 10$), bottom ($n = 9$)), UDSP-Hep ($n = 10$; 50 µg per mouse), anti-CTLA-4 ($n = 10$; 5 mg per kg) or anti-PD-1 ($n = 10$; 5 mg per kg), or UDSP-Hep combined with either antibody (top ($n = 10$), bottom ($n = 9$)). For **a**–**c** and **e**, data are mean ± s.e.m. Statistical analysis was performed using two-way ANOVA (**a**–**c** and **e**) and log-rank (Mantel–Cox) tests (**b** and **d**). Data are representative of three (**a**) or two (**b**–**e**) independent experiments.

MC38 tumours revealed marked enrichment of T and natural killer (NK) cells (Fig. 4d and Supplementary Fig. 3a). The frequencies of $CD8^+$ cells, including $GZMB^{hi}CD8^+$ T cells and NK cells ($GZMB^{hi}$ and $IFN\gamma^{hi}$ populations), greatly increased in tumour-infiltrating lymphocytes (TILs), whereas the ratio of regulatory T cells (T_{reg}) to $CD8^+$ T cells decreased (Fig. 4d and Extended Data Fig. 5h).

In B16F10-OVA and MC38 models, depletion of $CD8^+$ T cells, but not $CD4^+$ T cells and NK cells, abolished the antitumour effects of UDSP-Hep (Fig. 4e and Extended Data Fig. 6a,b). Consistently, UDSP-Hep was inactive in *Batf3*$^{-/-}$ mice lacking conventional type 1 DCs (cDC1s) ($CD103^+$ DCs and $CD8\alpha^+$ DCs)[32] (Fig. 4f). Priming of $CD8^+$ T cells by cDC1s occurred in the tdLNs. Accordingly, removal of the tdLNs in B16F10-OVA tumour-bearing mice blocked the antitumour activities of UDSP-Hep (Extended Data Fig. 6c,d). We further transferred naive OT-I $CD8^+$ T cells ($CD45.1^+$) into B16F10-OVA tumour-bearing mice ($CD45.2^+$); after PBS or UDSP-Hep treatment, $CD45.1^+CD44^+CD8^+$ T cells isolated from tdLNs were adoptively transferred into B16F10-OVA tumour-bearing *Cd8a*$^{-/-}$ mice. Mice receiving T cells from UDSP-Hep-treated donors, but not from PBS-treated donors, exhibited effective tumour control (Extended Data Fig. 6e,f and Supplementary Fig. 3b,c). Thus, UDSP-Hep induces priming and differentiation of specific tumouricidal $CD8^+$ T cells within the tdLNs.

UDSP-Hep remodulates the TME

In B16F10-OVA tumours, the percentage of activated NK cells among immune cells increased after UDSP-Hep treatment, whereas the percentage of $CD3^+$ T cells decreased slightly (Extended Data Fig. 5i). To better understand ALPK1-agonism-triggered antitumour immunity, we conducted scRNA-seq analysis of $CD45^+$ leukocytes within the TME of PBS or UDSP-Hep-treated B16F10-OVA tumours (Supplementary Fig. 4a). Clustering of sequenced cells identified 16 populations (Supplementary Fig. 4b,c). The ratio of lymphoid-derived to myeloid-derived cells markedly increased after UDSP-Hep treatment—NK cells showed the greatest increase (Supplementary Fig. 4d). Differential expression analysis of tumour-infiltrating immune cells revealed higher expression of genes encoding proinflammatory chemokines (*Ccl5* and *Xcl1*) and immune-cell adhesion molecules (*Icam1*, *Itgal*

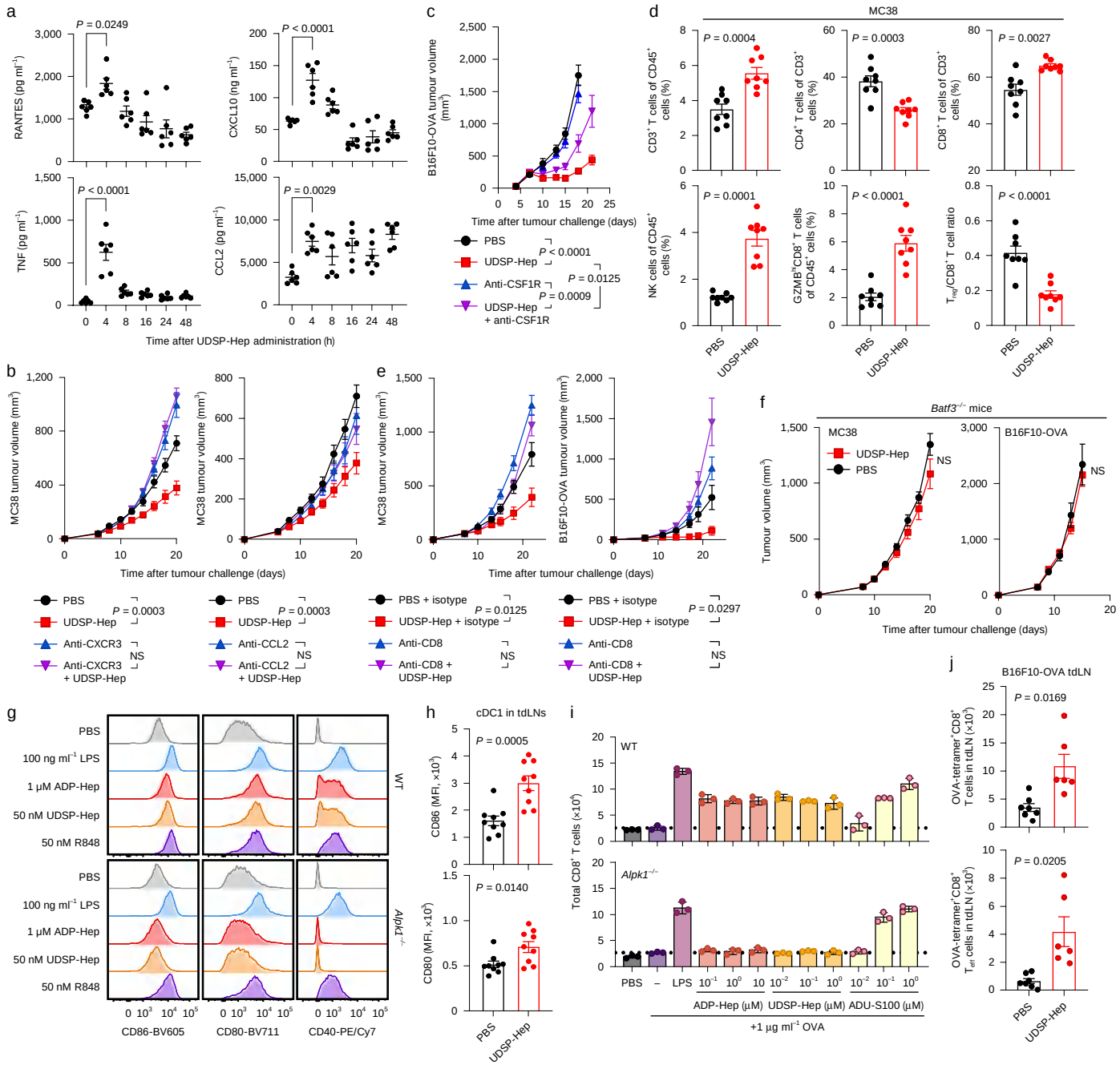

Fig. 4 | UDSP-Hep-induced antitumour immunity requires CXCL10 and CCL2 and features tumour-specific CD8⁺ T cell expansion through activation of DCs. a, Quantification of cytokines in UDSP-Hep-treated B16F10-OVA tumours. $n = 6$ mice per group. **b**, Growth curves of MC38 tumours in C57BL/6 mice treated with UDSP-Hep, CXCR3-blocking antibody, CCL2-neutralizing antibody or UDSP-Hep plus either antibody. $n = 12$ mice per group. **c**, Growth curves of B16F10-OVA tumours in C57BL/6 mice treated with UDSP-Hep alone or plus anti-CSF1R. $n = 10$ (anti-CSF1R) and $n = 9$ (other groups). **d**, Flow cytometry quantification of TILs in PBS- or UDSP-Hep-treated MC38 tumours. $n = 8$ mice per group. **e**, Growth curves of MC38 or B16F10-OVA tumours in C57BL/6 mice treated with PBS (left ($n = 9$), right ($n = 8$)), UDSP-Hep ($n = 9$), anti-CD8 depletion antibody (left ($n = 8$), right ($n = 9$)) or UDSP-Hep plus anti-CD8 ($n = 8$). **f**, Growth curves of MC38 ($n = 8$) or B16F10-OVA ($n = 7$) tumours in wild-type and *Batf3*$^{-/-}$ mice treated with PBS or UDSP-Hep. **g**, Histograms of anti-CD80, CD86 and CD40 staining of wild-type and *Alpk1*$^{-/-}$ iCD103-DCs treated with PBS or the indicated agonist. **h**, Median fluorescence intensity (MFI ± s.e.m.) of anti-CD86/CD80 staining of cDC1 cells from tdLNs of PBS- or UDSP-Hep-treated B16F10-OVA tumours. $n = 9$ mice per group. **i**, OT-I CD8⁺ cells were co-cultured with wild-type and *Alpk1*$^{-/-}$ iCD103-DCs that were prestimulated with OVA alone or with the indicated agonist. Flow cytometry quantification of total T cells is shown. Data are mean ± s.d. $n = 3$. **j**, Flow cytometry quantification of OVA-tet⁺CD44⁺CD8⁺ T cells (top) and OVA-tet⁺CD44⁺TOX⁻TCF1⁻ PD-1⁺CX3CR1⁺CD8⁺ effector T (T_{eff}) cells (bottom) in tdLNs of PBS-treated ($n = 7$) or UDSP-Hep-treated ($n = 6$) B16F10-OVA tumours. For **a**–**f**, **h** and **j**, data are mean ± s.e.m. Statistical analysis was performed using two-tailed unpaired Student's *t*-tests (**d** and **h**), Welch's *t*-tests (**d** and **j**), one-way ANOVA (**a**) and two-way ANOVA (**b**, **c**, **e** and **f**). All data are representative of three independent experiments.

and *Sell*) (Supplementary Fig. 4e), indicating immune-cell recruitment to the TME. In macrophages and myeloid-derived suppressor cells, expression of *Arg1* and *Spp1* (protumoural) was substantially lower in the UDSP-Hep-treated group (Supplementary Fig. 4f). T and NK cells showed higher expression of genes marking their activation (*Cd69* and *Klrk1*) or mediating their cytotoxicity (*Gzma*, *Gzmb*, *Prf1*

and *FasL*) (Supplementary Fig. 4g). Expression of lymphocyte survival and stemness maintenance genes (*Bcl2*, *Eomes* and *Tcf7*) also increased while those associated with T cell exhaustion (*Havcr2* and *Pdcd1*) decreased in UDSP-Hep-treated tumours (Supplementary Fig. 4h).

We further reclustered T cell and macrophage populations (Supplementary Fig. 5a,b,d,e). The proportions of *Spp1*$^+$ and *Tgm2*$^+$ tumour-promoting macrophages[33,34] were reduced by UDSP-Hep, whereas the proportions of *Il1b*$^+$ inflammatory macrophages and M1 macrophages were increased (Supplementary Fig. 5c). For T cells, the percentage of terminally exhausted CD8$^+$ cells decreased, while those of progenitor exhausted CD8$^+$ and effector CD8$^+$ cells increased (Supplementary Fig. 5f). Flow cytometry analysis of B16F10-OVA TILs confirmed the lowered ratio of PD-1$^+$ T cells among CD8$^+$ cells after UDSP-Hep treatment (Extended Data Fig. 6g and Supplementary Fig. 3d). Within PD-1$^+$CD8$^+$ T cells, the proportion of TCF1$^+$ progenitor exhausted cells increased while that of TIM-3$^+$ terminal exhausted cells decreased (Extended Data Fig. 6h,i). This indicates prolonged survival of tumour-infiltrating CD8$^+$ T cells and, therefore, an enhanced and sustained antitumour effect. These data highlight a shifting of the TME towards a proinflammatory, antitumoural state in UDSP-Hep-treated tumours.

DC activation and T cell expansion in tdLNs

cDC1s and CD8$^+$ T cells are both critical for UDSP-Hep-stimulated antitumour immunity. To examine this at a greater depth, cDC1s (CD103-expressing DCs, hereafter iCD103-DCs) were stimulated with ADP-Hep, UDSP-Hep, the TLR7/8 agonist R848 or LPS. R848 and both ALPK1 agonists stimulated expression of co-stimulatory markers (CD80, CD86 and CD40), and *Alpk1*$^{-/-}$ diminished the stimulation by ADP-Hep and UDSP-Hep (Fig. 4g and Extended Data Fig. 6j). Injection of UDSP-Hep into B16F10-OVA tumours also upregulated CD80 and CD86 in cDC1s in the tdLNs (Fig. 4h, Extended Data Fig. 6k and Supplementary Fig. 3e).

After co-culturing iCD103-DCs treated with ALPK1 agonist and OVA with naive OT-I CD8$^+$ T cells, notable expansion of the T cells was observed when the DCs were treated with ADP-Hep or a ten-fold lower concentration of UDSP-Hep (Fig. 4i). When transferring UDSP-Hep-activated iCD103-DCs into B16F10-OVA tumour-bearing mice (adjacent to tdLNs), we observed marked tumour control, resembling the effect of STING-agonist-primed iCD103-DCs (Extended Data Fig. 6l). Supporting the antitumour T cell activation effect of UDSP-Hep-primed cDC1s, the proportion of CD69$^+$ T cells among CD8$^+$ (also CD4$^+$) populations in the tdLNs of B16F10-OVA tumours increased greatly after UDSP-Hep treatment (Extended Data Fig. 6m,n and Supplementary Fig. 3a). OVA-tetramer staining revealed an evident increase in tumour-specific CD8$^+$ T cells and effector CD8$^+$ T cells (Fig. 4j and Supplementary Fig. 3f). Thus, UDSP-Hep stimulates DCs to activate antigen-specific CD8$^+$ T cells in the tdLNs.

Differentiation from STING/TLR agonists

Lastly, we compared UDSP-Hep with other innate immune agonists. Profiling 73 cell lines (NCI-60 non-immune plus 13 immune cells) revealed a broad expression of ALPK1/TIFA (Extended Data Fig. 7). By contrast, TLR7/8/9 expression was restricted to haematopoietic/lymphoid cells; STING expression showed an intermediate range, being relatively lower in non-immune cells. In THP-1 cells (or RPMI-8226 B lymphocytes) that expressed ALPK1, STING and TLR7, distinct cytokine profiles emerged after stimulation with their cognate agonists (Extended Data Fig. 8a,b and Supplementary Fig. 6). Dose-titration and time-course analyses in BMDMs revealed notable differences in the cytokine signatures of the three pathways (Supplementary Fig. 7). Injecting each of the three agonists into mice induced featured cytokines besides a common set of ones (Extended Data Fig. 8c and Supplementary Fig. 8). UDSP-Hep strongly induced CXCL1 and CXCL2, R848 preferentially upregulated IL-9 and IL-22, and the STING agonist ADU-S100 generated the highest levels of IL-6, IL-27, CCL4 and TNF.

Injection of the mouse STING agonist DMXAA[35] into B16F10 tumours had marginal antitumour effects but resulted in efficient tumour control after UDSP-Hep co-injection (Extended Data Fig. 9a–c). A similar synergistic effect was observed with the clinical-stage STING agonist ADU-S100[36] (Fig. 5a). Synergetic or additive effects were also noted after co-administration of R848 and UDSP-Hep in the B16F10 and MC38 models (Extended Data Fig. 9d,e). Thus, the antitumour mechanism of UDSP-Hep is differentiated from those of the other agonists. Supporting this, anti-CCL2 did not affect the efficacy of TLR7/8 and STING agonists in the MC38 model, whereas anti-CXCR3 remained effective for these two types of agonists (Extended Data Fig. 9f,g). In PBMCs, UDSP-Hep, ADU-S100 and 41c-A (a TLR7-specific agonist from Roche) all induced robust production of CXCL10; the effects of TLR7 and STING agonists peaked at a certain dose and then decreased, whereas UDSP-Hep showed a normal dosage effect (Extended Data Fig. 10a). Notably, the relative ability of UDSP-Hep to induce IL-6 and TNF (underlying the toxicity of TLR7/STING agonists), compared with that of TLR7 or STING agonist, was markedly lower (Extended Data Fig. 10a), indicating a potential advantage in ALPK1 agonists.

In B16F10-OVA cells, UDSP-Hep dose-dependently promoted MHC class I presentation of the SIINFEKL epitope while ADU-S100 showed no such effects (Fig. 5b). Both UDSP-Hep and ADU-S100 could stimulate cDC1 cells to cross-prime CD8$^+$ T cells, but the minimal concentration required for UDSP-Hep was ten times lower than that for ADU-S100 (Fig. 4i). The same difference was observed in the cDC1-activation assay (Fig. 5c and Extended Data Fig. 10b). In macrophages, UDSP-Hep and ADU-S100 but not R848 elevated CD86 expression (Extended Data Fig. 10c,d). The UDSP-Hep-treated macrophages robustly induced OT-I T cell proliferation to a much stronger extent than R848- or ADU-S100-treated cells (Extended Data Fig. 10e,f). In contrast to ADU-S100, which can induce T cell apoptosis[37,38], UDSP-Hep and R848 caused no evident apoptosis in activated mouse splenic CD3$^+$ T cells (Extended Data Fig. 10g).

UDSP-Hep efficiently eliminated Hepa 1-6 tumours with a durable memory, whereas DMXAA was ineffective (Fig. 3b and Extended Data Fig. 10h). A greater proportion of tumour-specific memory T (T_{tsm}) cells was detected in the tdLNs and spleen of UDSP-Hep-treated mice compared with in control or DMXAA-treated mice bearing the same Hepa 1-6 tumours (Fig. 5d–f and Supplementary Fig. 3f). After tumour clearance by UDSP-Hep, high-level T_{tsm} populations were detected in the tdLNs, non-tdLNs, spleen and the tumour-injection site (Extended Data Fig. 9h,i). B16F10-OVA tumours were sensitive to both ALPK1 and STING agonists, and comparable increases in the frequency of tumour-specific effector CD8$^+$ T cells within the tdLNs were observed (Fig. 5g). UDSP-Hep and DMXAA co-treatment elicited a much greater expansion of these effector T cells (Fig. 5g), echoing the functional cooperation between the two agonists (Extended Data Fig. 9a–c). Despite this, UDSP-Hep, compared with DMXAA, induced a substantially higher percentage of T_{tsm} cells (Fig. 5g), the targets of the anti-PD-1 checkpoint blockade[39].

Thus, ALPK1-agonist-induced antitumour immunity has multifaceted mechanistic differentiations from that of STING and other immune agonists. The prominent ability in UDSP-Hep to promote protective memory T cell differentiation without causing cell death indicates another possible advantage of ALPK1 agonism over STING agonism.

Discussion

Here we establish that ALPK1 agonism could stimulate CD8$^+$ T-cell-mediated antitumour immunity and synergize with ICIs. The antitumour immunity requires macrophages and cDC1s as well as ALPK1-induced CXCL10/CCL2. ALPK1 agonists can act on DCs and stimulate cross-presentation, resulting in the activation and expansion

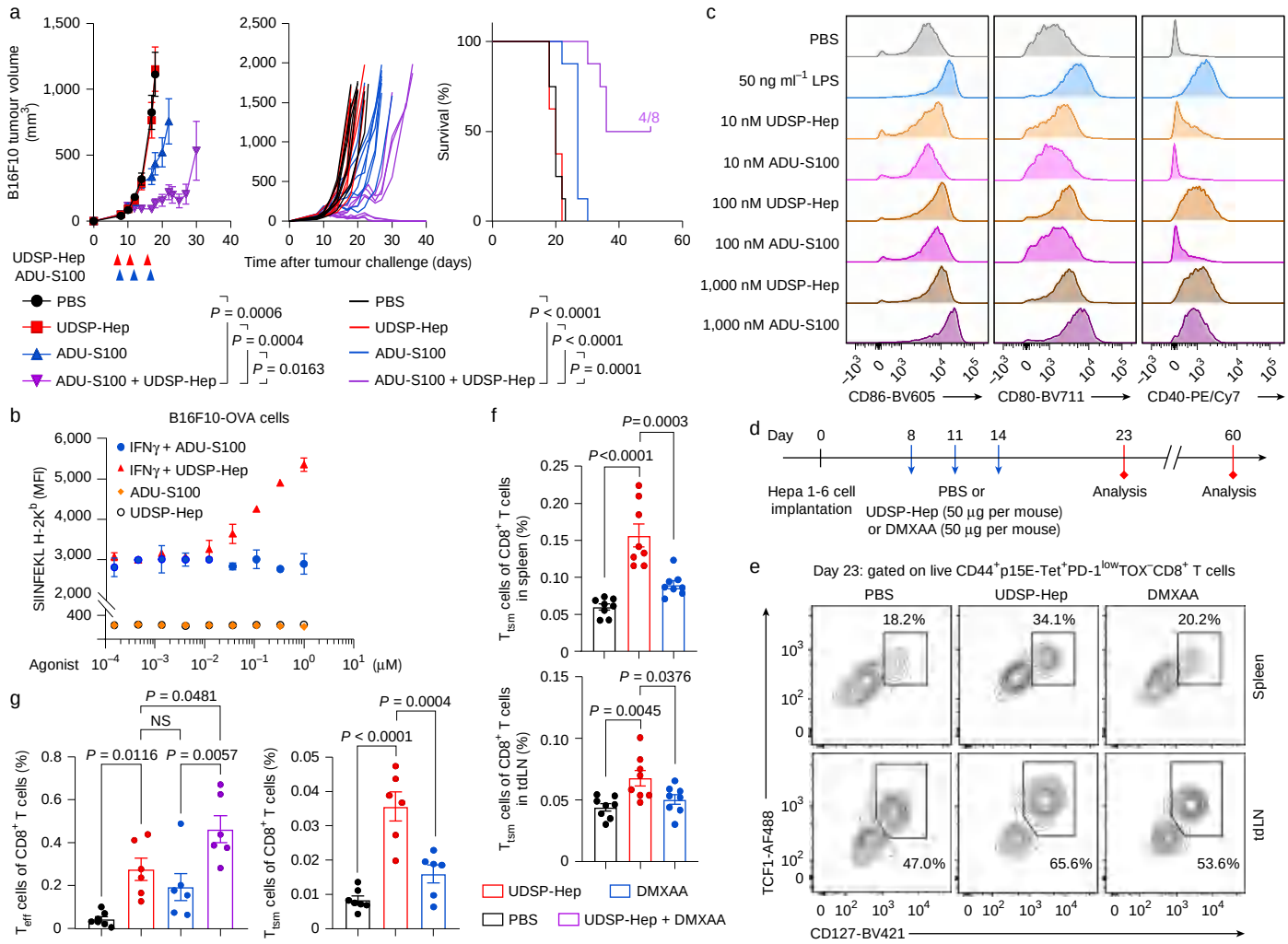

Fig. 5 | UDSP-Hep can synergize with STING agonist owing to their differential antitumour immune features. a, Average (left) and individual animal (middle) tumour growth curves and mouse survival (right) of native B16F10 tumours treated with PBS, UDSP-Hep (100 μg per mouse), ADU-S100 (25 μg per mouse) or UDSP-Hep combined with ADU-S100. The fraction of surviving mice is shown. Data are mean ± s.e.m. $n = 8$ mice per group. **b**, IFNγ-induced (1 ng ml^{-1}) antigen presentation on B16F10-OVA cells treated with increasing doses of UDSP-Hep or ADU-S100. The mean ± s.d. fluorescence intensity of anti-SIINFEKL–H-2K^b staining is shown. **c**, Histograms of anti-CD86, CD80 and CD40 staining of purified iCD103-DCs treated with PBS, LPS, UDSP-Hep or ADU-S100. **d**–**f**, Hepa-1-6-tumour-bearing mice were treated with PBS, UDSP-Hep or DMXAA, and TCF1$^+$CD127$^+$CD8$^+$ T_{tsm} cells were then measured. **d**, Schematic of the experiment. **e**,**f**, T_{tsm} cells in spleen and tdLNs on day 23. **e**, Representative flow cytometry plots gated on T_{tsm} cells. **f**, Quantification of T_{tsm} cells among CD8$^+$ T cells. Data are mean ± s.e.m. $n = 8$ mice per group. The day-60 data are shown in Extended Data Fig. 9h,i. **g**, Flow cytometry quantification of effector T cells (left) and T_{tsm} cells (right) in the tdLNs of B16F10-OVA-tumour-bearing mice treated with PBS, UDSP-Hep (50 μg per mouse), DMXAA (50 μg per mouse) or UDSP-Hep combined with DMXAA. Data are mean ± s.e.m. $n = 7$ (PBS) and $n = 6$ (other groups). Statistical analysis was performed using two-way ANOVA (**a**, left), log-rank (Mantel–Cox) tests (**a**, right) and one-way ANOVA (**f** and **g**). Data are representative of two (**a**) or three (**b**–**g**) independent experiments.

of tumour-specific T cells. Given the wide presence of the ALPK1 pathway in immune and non-immune cells, future studies shall assess the contributions of different cell types in remodulating the TME.

Activation of innate immunity holds promise in cancer immunotherapies. Extensive efforts are being undertaken to target the STING and TLR pathways, but their agonists encounter difficulties in humans. As antiviral defences, STING and TLR7/8/9 instigate antitumour effects largely through activating IFN signalling[40]. However, prolonged exposure to IFNs may cause immunosuppression; recent clinical trials indeed show that inhibition of IFN signalling instead enhances the efficacy of anti-PD-1 therapy[41,42]. Bacteria-induced responses have long been linked to anticancer therapy, dating back to the use of Corey's toxins a century ago. The BCG vaccine is widely used to treat bladder cancers[43,44]. ALPK1 activation by its bacteria-derived agonists stimulates an inflammatory profile distinct from those of TLR/STING activation. ALPK1 agonists can also synergize with STING or TLR agonists. The ALPK1 axis differs from the STING pathway in several aspects, including its broader expression in different cell types. ALPK1 agonism further differs from STING agonism in stimulating tumour-cell antigen presentation, macrophage–DC cross-priming and protective memory T cell differentiation, but does not induce T cell apoptosis.

A recent study showed that disease-causing ALPK1 mutants can respond to UDP-mannose, ADP-ribose and cyclic ADP-ribose[45]. Here we find that diverse nucleotide-conjugated heptoses can activate ALPK1 with UDP-Hep being the most potent one. UDP-Hep distinguishes ALPK1(C57BL/6) from ALPK1(129), correlating with mouse susceptibility to bacteria-associated colitis[9–12]. Thus, the pathophysiological function of ALPK1 may not be limited to sensing of ADP-Hep; ALPK1 may recognize other sugar nucleotides of foreign origin or even endogenous sources.

Online content

Any methods, additional references, Nature Portfolio reporting summaries, source data, extended data, supplementary information,

acknowledgements, peer review information; details of author contributions and competing interests; and statements of data and code availability are available at https://doi.org/10.1038/s41586-025-09828-9.

1. Ribas, A. et al. SD-101 in combination with pembrolizumab in advanced melanoma: results of a phase Ib, multicenter study. *Cancer Discov.* **8**, 1250–1257 (2018).
2. Ackerman, S. E. et al. Immune-stimulating antibody conjugates elicit robust myeloid activation and durable antitumor immunity. *Nat. Cancer* **2**, 18–33 (2021).
3. Ramanjulu, J. M. et al. Design of amidobenzimidazole STING receptor agonists with systemic activity. *Nature* **564**, 439–443 (2018).
4. Pan, B. S. et al. An orally available non-nucleotide STING agonist with antitumor activity. *Science* **369**, eaba6098 (2020).
5. Zhou, P. et al. Alpha-kinase 1 is a cytosolic innate immune receptor for bacterial ADP-heptose. *Nature* **561**, 122–126 (2018).
6. Zimmermann, S. et al. ALPK1- and TIFA-dependent innate immune response triggered by the *Helicobacter pylori* type IV secretion system. *Cell Rep.* **20**, 2384–2395 (2017).
7. Milivojevic, M. et al. ALPK1 controls TIFA/TRAF6-dependent innate immunity against heptose-1,7-bisphosphate of gram-negative bacteria. *PLoS Pathog.* **13**, e1006224 (2017).
8. Williams, L. B. et al. *ALPK1* missense pathogenic variant in five families leads to ROSAH syndrome, an ocular multisystem autosomal dominant disorder. *Genet. Med.* **21**, 2103–2115 (2019).
9. Boulard, O., Kirchberger, S., Royston, D. J., Maloy, K. J. & Powrie, F. M. Identification of a genetic locus controlling bacteria-driven colitis and associated cancer through effects on innate inflammation. *J. Exp. Med.* **209**, 1309–1324 (2012).
10. Ryzhakov, G. et al. Alpha kinase 1 controls intestinal inflammation by suppressing the IL-12/Th1 axis. *Nat. Commun.* **9**, 3797 (2018).
11. Buettner, M. & Bleich, A. Mapping colitis susceptibility in mouse models: distal chromosome 3 contains major loci related to *Cdcs1*. *Physiol. Genom.* **45**, 925–930 (2013).
12. Ermann, J. et al. Severity of innate immune-mediated colitis is controlled by the cytokine deficiency-induced colitis susceptibility-1 (*Cdcs1*) locus. *Proc. Natl Acad. Sci. USA* **108**, 7137–7141 (2011).
13. Corrales, L., Matson, V., Flood, B., Spranger, S. & Gajewski, T. F. Innate immune signaling and regulation in cancer immunotherapy. *Cell Res.* **27**, 96–108 (2017).
14. Demaria, O. et al. Harnessing innate immunity in cancer therapy. *Nature* **574**, 45–56 (2019).
15. Tang, Y. et al. The beta-D-manno-heptoses are immune agonists across kingdoms. *Science* **385**, 678–684 (2024).
16. Cui, J. et al. The ALPK1 pathway drives the inflammatory response to *Campylobacter jejuni* in human intestinal epithelial cells. *PLoS Pathog.* **17**, e1009787 (2021).
17. Faass, L., Hauke, M., Stein, S. C. & Josenhans, C. Innate immune activation and modulatory factors of *Helicobacter pylori* towards phagocytic and nonphagocytic cells. *Curr. Opin. Immunol.* **82**, 102301 (2023).
18. Pfannkuch, L. et al. ADP heptose, a novel pathogen-associated molecular pattern identified in *Helicobacter pylori*. *FASEB J.* **33**, 9087–9099 (2019).
19. Martin-Gallausiaux, C. et al. *Akkermansia muciniphila* upregulates genes involved in maintaining the intestinal barrier function via ADP-heptose-dependent activation of the ALPK1/TIFA pathway. *Gut Microbes* **14**, 2110639 (2022).
20. Martin-Gallausiaux, C. et al. Fusobacterium nucleatum promotes inflammatory and anti-apoptotic responses in colorectal cancer cells via ADP-heptose release and ALPK1/TIFA axis activation. *Gut Microbes* **16**, 2295384 (2024).
21. Kozycki, C. T. et al. Gain-of-function mutations in *ALPK1* cause an NF-κB-mediated autoinflammatory disease: functional assessment, clinical phenotyping and disease course of patients with ROSAH syndrome. *Ann. Rheum. Dis.* **81**, 1453–1464 (2022).
22. Jamilloux, Y. et al. *ALPK1* gene mutations drive autoinflammation with ectodermal dysplasia and progressive vision loss. *J. Clin. Immunol.* **41**, 1671–1673 (2021).
23. Zhong, L. et al. Juvenile onset splenomegaly and oculopathy due to germline mutation in *ALPK1*. *J. Clin. Immunol.* **40**, 350–358 (2020).
24. Sun, Z. et al. Ocular manifestations of ROSAH syndrome caused by different mutations of the *ALPK1* gene. *Am. J. Ophthalmol.* **281**, 456–464 (2025).
25. Sangiorgi, E. et al. Rare missense variants in the ALPK1 gene may predispose to periodic fever, aphthous stomatitis, pharyngitis and adenitis (PFAPA) syndrome. *Eur. J. Hum. Genet.* **27**, 1361–1368 (2019).
26. Luster, A. D. & Leder, P. IP-10, a -C-X-C- chemokine, elicits a potent thymus-dependent antitumor response in vivo. *J. Exp. Med.* **178**, 1057–1065 (1993).
27. Pertl, U. et al. IFN-γ-inducible protein-10 is essential for the generation of a protective tumor-specific CD8 T cell response induced by single-chain IL-12 gene therapy. *J. Immunol.* **166**, 6944–6951 (2001).
28. Dufour, J. H. et al. IFN-γ-inducible protein 10 (IP-10; CXCL10)-deficient mice reveal a role for IP-10 in effector T cell generation and trafficking. *J. Immunol.* **168**, 3195–3204 (2002).
29. Nakasone, Y. et al. Host-derived MCP-1 and MIP-1alpha regulate protective anti-tumor immunity to localized and metastatic B16 melanoma. *Am. J. Pathol.* **180**, 365–374 (2012).
30. Lanca, T. et al. Protective role of the inflammatory CCR2/CCL2 chemokine pathway through recruitment of type 1 cytotoxic gammadelta T lymphocytes to tumor beds. *J. Immunol.* **190**, 6673–6680 (2013).
31. Deshmane, S. L., Kremlev, S., Amini, S. & Sawaya, B. E. Monocyte chemoattractant protein-1 (MCP-1): an overview. *J. Interferon Cytokine Res.* **29**, 313–326 (2009).
32. Hildner, K. et al. *Batf3* deficiency reveals a critical role for $CD8\alpha^+$ dendritic cells in cytotoxic T cell immunity. *Science* **322**, 1097–1100 (2008).
33. Bill, R. et al. CXCL9: SPP1 macrophage polarity identifies a network of cellular programs that control human cancers. *Science* **381**, 515–524 (2023).
34. Afik, R. et al. Tumor macrophages are pivotal constructors of tumor collagenous matrix. *J. Exp. Med.* **213**, 2315–2331 (2016).
35. Conlon, J. et al. Mouse, but not human STING, binds and signals in response to the vascular disrupting agent 5,6-dimethylxanthenone-4-acetic acid. *J. Immunol.* **190**, 5216–5225 (2013).
36. Meric-Bernstam, F. et al. Phase I dose-escalation trial of MIW815 (ADU-S100), an intratumoral STING agonist, in patients with advanced/metastatic solid tumors or lymphomas. *Clin. Cancer Res.* **28**, 677–688 (2022).
37. Gulen, M. F. et al. Signalling strength determines proapoptotic functions of STING. *Nat. Commun.* **8**, 427 (2017).
38. Larkin, B. et al. Cutting edge: activation of STING in T cells induces type I IFN responses and cell death. *J. Immunol.* **199**, 397–402 (2017).
39. Huang, Q. et al. The primordial differentiation of tumor-specific memory $CD8^+$ T cells as bona fide responders to PD-1/PD-L1 blockade in draining lymph nodes. *Cell* **185**, 4049–4066 (2022).
40. Vitiello, G. A. F., Ferreira, W. A. S., Cordeiro de Lima, V. C. & Medina, T. D. S. Antiviral responses in cancer: boosting antitumor immunity through activation of interferon pathway in the tumor microenvironment. *Front. Immunol.* **12**, 782852 (2021).
41. Zak, J. et al. JAK inhibition enhances checkpoint blockade immunotherapy in patients with Hodgkin lymphoma. *Science* **384**, eade8520 (2024).
42. Mathew, D. et al. Combined JAK inhibition and PD-1 immunotherapy for non-small cell lung cancer patients. *Science* **384**, eadf1329 (2024).
43. Morales, A., Eidinger, D. & Bruce, A. W. Intracavitary *Bacillus* Calmette-Guerin in the treatment of superficial bladder tumors. *J. Urol.* **116**, 180–183 (1976).
44. Babjuk, M. et al. EAU guidelines on non-muscle-invasive urothelial carcinoma of the bladder, the 2011 update. *Eur. Urol.* **59**, 997–1008 (2011).
45. Snelling, T., Saalfrank, A., Wood, N. T. & Cohen, P. ALPK1 mutants causing ROSAH syndrome or Spiradenoma are activated by human nucleotide sugars. *Proc. Natl Acad. Sci. USA* **120**, e2313148120 (2023).

Methods

Antibodies

Antibodies against ALPK1 (ab236626), TIFA (ab239352), phospho-T9 TIFA (ab214815 and a custom-made polyclone), TLR7 (ab124928) and MYC tag (ab32) were obtained from Abcam. Antibodies against STING (13647), TLR8 (11886) and TLR9 (13674) were purchased from Cell Signaling Technology. Antibodies against α-tubulin (T5168) and Flag (M2) were from Sigma-Aldrich. Antibodies against eGFP (11814460001) were obtained from Roche. For western blotting, horseradish peroxidase (HRP)-conjugated goat anti-mouse IgG (AS003) and HRP-conjugated goat anti-rabbit IgG (AS014) antibodies were purchased from ABclonal.

The following fluorochrome-conjugated antibodies were used in the flow cytometry analysis: anti-H-2Kb bound to SIINFEKL antibody (25-D1.16, BioLegend), anti-mouse CD16/32 (BioLegend, 101302), T-Select H-2Kb OVA Tetramer-SIINFEKL-APC (MBL, TS-M501-2C), T-Select H-2Kb MuLV p15E Tetramer-KSPWFTTL-APC (MBL, TS-M507-2), anti-mouse CD103 (2E7, BioLegend), CD127 (A7R34, BioLegend), CD11b (M1/70, BioLegend), CD11c (N418, BioLegend), CD279 (PD-1, RMP1-14 or 29F.1A12, BioLegend), CD3 (17A2, BioLegend), TIM-3 (RMT3-23, BioLegend), CD4 (GK1.5, BioLegend), CD40 (3/23, BioLegend), CD44 (IM7, BioLegend), CD45 (30-F11, BioLegend), CD45.1 (A20, BioLegend), CD62L (MEL-14, BioLegend), CD69 (H1.2F3, BioLegend), CD80 (16-10A1, BioLegend), CD86 (GL-1, BioLegend), CD8α (53-6.7, BioLegend), CX3CR1 (SA011F11, BioLegend), I-A/I-E (M5/114.15.2, BioLegend), F4/80 (BM8, BioLegend), FOXP3 (MF-14, BioLegend), granzyme B (QA16A02, BioLegend), IFNγ (XMG1.2, BioLegend), NK1.1 (PK136, BioLegend), TCF1/TCF7 (C63D9, Cell Signaling Technology) and TOX (TXRX10, Invitrogen).

Checkpoint inhibitors including anti-PD-1 were provided by BeiGene; anti-CTLA-4, anti-4-1BB and anti-PD-L1 were supplied by Adagene. For cytokine blocking or cell depletion assays, anti-mouse CXCR3 (CXCR3-173), CCL2 (2H5), CD4 (GK1.5), CD8α (2.43), NK1.1 (PK136) and isotype control (LTF-2) antibodies were purchased from BioXCell. Anti-CSF1R (AFS98) was obtained from BioLegend. Anti mouse-CD8α was sourced from the Antibody Centre of NIBS.

Compounds and compound synthesis

Methods for synthesizing ADP-Hep and its analogues listed in Extended Data Fig. 2 are described in detail in Supplementary Data 1. DMXAA was purchased from Invivogen (tlrl-dmx). ADU-S100 (HY-12885B), R848 (HY-13740) and cyclophosphamide (HY-17420) were from MedChem Express. LPS (L4130) and 4′,6-diamidino-2-phenylindole (DAPI, D9542) were purchased from Sigma-Aldrich. Imject Alum was purchased from Thermo Fisher Scientific (77161). The TLR7-specific agonist (compound 41c-A) used in PBMC experiments is a RO7020531 derivate and was synthesized according to the patent WO2019166432A1. PTx was purchased from List Biological Laboratories (180) and Ginsenoside Rb1 (CSN19503-002) was from Npharm.

Cell culture, cell viability and NF-κB luciferase reporter assays

The B16F10 (CRL-6475), 4T1 (CRL-2539), HEK293T (CRL-3216), THP-1 (TIB-202), Toledo (CRL-2631), NALM6, G5 (CRL-3273), MV-4-11 (CRL-9591), Hep G2 (HB-8065), Hep 3B (HB-8064), Ca Ski (CRL-1550), SiHa (HTB-35) and ARPE-19 (CRL-2302) cell lines were purchased from American Type Culture Collection (ATCC). The NOMO-1 (CBP60515), OCI-AML2 (CBP60527), OCI-AML-3 (CBP60817) and MOLM-13 (CBP60678) cell lines were purchased from Nanjing Kebai Biotechnology. The Huh7 (SCSP-526) cell line was purchased from Cell Bank of Chinese Science Academy. The E0771 mammary carcinoma cell line (Delf-17882) was purchased from Hefei Wanwu Biotechnology. The MC38 colon adenocarcinoma and the Hepa 1-6 hepatoma cell lines were gifts from BeiGene and Pyrotech Biotechnology, respectively. The MB49 urothelial carcinoma cell line was a gift from X. Zhang. The NCI-60 panel of cancer cells (including RPMI-8226) was obtained from the Development Therapeutic Program at the National Cancer Institute and cultured according to the instructions provided. HEK293T cells stably expressing eGFP–TIFA and *ALPK1*$^{-/-}$ HEK293T cells were generated previously[5]. B16F10 and 4T1 cells were lentivirally transduced to express OVA. B16F10, 4T1, THP-1, RPMI-8226, Huh7, Toledo, NALM6 clone G5, MV-4-11, Ca Ski, NOMO-1, OCI-AML2, OCI-AML3, MOLM-13 and NCI-60 cancer cells were cultured in RPMI 1640 (Gibco, C22400500BT) supplemented with 10% (v/v) FBS and 2 mM L-glutamine (Gibco, 25030-081). HEK293T, MC38, MB49, SiHa and E0771 cells were cultured in DMEM (Gibco, C11965500BT) supplemented with 10% FBS and 2 mM L-glutamine. Hepa 1-6 cells were cultured in DMEM supplemented with 10% FBS, 2 mM L-glutamine and 1 mM sodium pyruvate (Gibco,11360-070). ARPE-19 cells were cultured in DMEM/F12 (Gibco, 11320-033) supplemented with 10% (v/v) FBS and 2 mM L-glutamine. Hep G2 and Hep 3B cells were cultured in EMEM (Sigma-Aldrich, M4655) supplemented with 10% (v/v) FBS and 2 mM L-glutamine. All cells were grown in a 5% CO_2 incubator at 37 °C. The identity of Hepa 1-6 and E0771 cells was validated by short-tandem-repeat (STR) profiling and that of other cells was frequently checked by their morphological features but had not been authenticated by STR. All cell lines were routinely tested for mycoplasma contamination.

For viability assays, cells were seeded into 96-well plates and treated with varying concentrations of ADP-Hep or UDSP-Hep for 24 h. Cell viability was assessed using the Cell Counting Kit-8 (CCK-8; MedChem Express, HY-K0301) according to the manufacturer's instructions. For serum-deprivation experiments, culture plates were precoated with 0.01% poly-L-lysine (Sigma-Aldrich, P8920) to prevent detachment under serum-free conditions. For NF-κB luciferase reporter assay, plasmids were transfected into HEK293T cells using JetPRIME (Polyplus Transfection) according to the manufacturer's recommended protocols. After transfection for 12 h, the indicated ALPK1 agonist was electroporated into the cells or added directly to the cell culture medium; the stimulation was allowed to proceed for 8 h. Luciferase activity was quantified using the Dual Luciferase Reporter Assay System (Promega, E1960).

For T cell viability assays, splenic T cells were isolated using the MojoSort mouse CD3 T cell isolation kit (BioLegend, 480024) and then activated for 24 h in T cell medium (TCM, RPMI 1640 containing 10% heat-inactivated FBS, 100 U ml^{-1} penicillin–streptomycin, 1× MEM NEAA, 25 mM HEPES, 1 mM sodium pyruvate, 2 mM L-glutamine and 55 μM 2-mercaptoethanol) containing 0.25 μg ml^{-1} anti-CD3ε (145-2C11, BioLegend), 1 μg ml^{-1} anti-CD28 (37.51, BioLegend) and 20 U ml^{-1} IL-2 (Novoprotein, C013) in plates precoated with goat anti-Armenian hamster IgG (Invitrogen, 31115). After activation, agonists were administered, followed by incubation for an additional 24 h. Viability was quantified by Annexin V-FITC/PI staining (Beyotime, C1062L) using flow cytometry.

Recombinant protein purification

Recombinant human apo-ALPK1 protein was purified using the Bac-to-Bac Baculovirus Expression System (Life Technologies) according to the manufacturer's protocol. Initially, Sf9 insect cells were cultured in Sf-900 II SFM at a density ranging from 5×10^5 to 2×10^6 cells per ml. Bacmids carrying twin strep-TEV site-ALPK1 were transfected into Sf9 cells using CellFECTIN II reagent to initiate recombinant baculovirus production. Then, 1 l of cells (1.6×10^6 cells per ml) was then infected with 10 ml of the P3 baculovirus and cultured at 28 °C for 72 h to achieve large-scale expression. Cells were collected by centrifugation at 1,000*g*, resuspended in lysis buffer comprising 20 mM Tris-HCl (pH 8.0), 500 mM NaCl, 10% glycerol and a complete EDTA-free protease inhibitor cocktail (Roche, 04693132001), and subsequently lysed using an ultrasonic cell disruptor. The ALPK1 protein was subjected to affinity purification using Strep-Tactin agarose beads (IBA, 6-6350-025). The Strep tag was removed by homemade tobacco etch virus protease at 4 °C, after which the protein was purified by Superdex 200 Increase 10/300 GL gel-filtration chromatography (GE Healthcare Life Sciences).

In vitro kinase assay and intracellular assessment of ALPK1 agonists

The activity of ALPK1 was assessed according to reported procedures[5]. In brief, 35 nM recombinant human ALPK1 was incubated with 250 μM TIFA 1–19 amino acid peptide substrate in a 50 μl of reaction (45 mM HEPES, pH 7.4 and 4 mM $MgCl_2$). ADP-Hep and UDSP-Hep were titrated across a concentration gradient to assess ALPK1 activation. The kinase reaction was initiated by adding 700 μM ATP, followed by incubation at 30 °C for 60 min. ADP production was measured using the ADP-Glo Kinase Assay kit (Promega, V9101).

To assess the activity of ALPK1 agonists in cells, native or *ALPK1*$^{-/-}$ HEK293T cells expressing eGFP–TIFA from the genome were treated with the indicated agonist for 2 h. Cells were collected; TIFA phosphorylation was probed by immunoblotting using the anti-pT9-TIFA. To compare the activity of ALPK1 from different mouse strains, *Alpk1* cDNA was constructed into the pCS2-3×Flag vector, and the plasmid was transfected into *ALPK1*$^{-/-}$ eGFP–TIFA-expressing HEK293T cells. After agonist treatment, cell lysates were subjected to immunoblotting. All immunoblotting analyses were conducted at least three times, and representative blots are presented in relevant figures.

Transcriptional profiling by RNA-seq analysis

Primary BMDMs from wild-type or *Alpk*$^{-/-}$ mice were prepared according to a standard protocol[46]. THP-1 and RPMI-8226 cells were treated with varying concentrations of ADP-Hep, UDSP-Hep, R848 or ADU-S100 for 4 h. BMDMs were treated with 100-μM ADP-Hep for 4 h. Total RNA was extracted using an RNA extraction kit (Vazyme, RC112-01) according to the manufacturer's instructions. For THP-1 and RPMI-8226 cells, RNA libraries were prepared using VAHTS mRNA Capture Beads (N401) and the VAHTS Universal V8 RNA-seq Library Prep Kit for Illumina NR605-02 (Vazyme), and sequencing was performed on the Illumina NovaSeq X Plus instrument. For BMDMs, Illumina-barcoded libraries were prepared using the Illumina Stranded mRNA Prep, Ligation kit (20040534), and sequenced on the Illumina NextSeq 2000 instrument using single-read 100 bp. RNA-seq data were quality-controlled in trim-galore (v.0.6.10); low-quality reads, adapter sequences, and reads shorter than 30 bp were removed. Cleaned reads were aligned to the reference genome mm10 using the STAR (Spliced Transcripts Alignment to a Reference) tool (v.2.7.10a). FeatureCounts (v.2.0.6) was used to quantify gene expression levels from the aligned BAM files and read counts for each gene were obtained. The heat map of gene expression across samples was generated using the pheatmap (v.1.0.12) package in R.

Mice

Wild-type C57BL/6, 129 and BALB/c mice were purchased from Vital River Laboratory Animal Technology. NSG mice were from BIOCYTOGEN. *Alpk1*$^{-/-}$ and *Alpk1*$^{T237M/T237M}$ mice were generated previously[5,21]. *Batf3*$^{-/-}$ mice were provided by X. Xia. The *Cd8a*$^{-/-}$ mice were supplied by L. Ye. CD45.1 transgenic mice and OT-I mice were provided by M. Xu. *ALPK1*-humanized mice were supplied by Pyrotech Biotechnology. All of the mice were maintained in the specific-pathogen-free facility at the National Institute of Biological Sciences, Beijing. All of the mouse experiments were performed in accordance with the national guidelines for housing and care of laboratory animals (Ministry of Health, China) and the protocol is in accordance with institutional regulations after review and approval by the Institutional Animal Care and Use Committee at National Institute of Biological Sciences, Beijing. Euthanasia was conducted on the designated day using CO_2 inhalation.

Tumour challenge and analysis of tumour growth

For syngenetic tumour models, C57BL/6, BALB/c mice or NSG mice, aged 6–8 weeks, were used. The number of cells inoculated into one mouse was 2×10^5 for B16F10 and 4T1-OVA, 3×10^6 for Hepa 1-6 and 1×10^6 for B16F10-OVA, MC38, MB49 and E0771. The cells (in PBS) were injected subcutaneously (unless otherwise specified) into the mice on day 0. As indicated, 4T1-OVA and E0771 breast cancer cells were orthotopically implanted into the mammary fat pad of the fourth mammary gland. Mice were anaesthetized with isoflurane (2% in oxygen) by inhalation. After inoculation, mice with comparable tumour burdens were randomly allocated to distinct treatment cohorts. The indicated amounts of ADP-Hep or UDSP-Hep or the PBS control were intratumourally administered into the mice on the specified dates. Tumour progression was monitored at regular intervals of 2–3 days using digital callipers. The tumour volume was computed using the formula: volume = (length × width^2)/2. Criteria delineating end-point events included the presence of a progressively enlarging tumour reaching 20 mm in its longest dimension, a tumour volume surpassing 1,500 mm^3 (for survival analyses) or 2,000 mm^3 (for other experiments), or ulceration/necrosis manifestation within the tumour.

To examine the distal effect of tumour control, 3×10^6 Hepa 1-6 cells, 1×10^6 B16F10-OVA cells or 2×10^6 MC38 cells were inoculated into the right flank of each mouse, and 1.5×10^6 Hepa 1-6 cells or 0.5×10^6 B16F10-OVA or MC38 cells were inoculated into the left flank of the respective mouse. On day 7, mice were randomly assigned to receive either PBS or UDSP-Hep treatment (intratumoural injection) on the right side. Tumour growth on both sides was monitored as above described. For combination therapies, mice were administered intraperitoneally with the indicated ICIs or intratumoural injections of the TLR7 agonist R848 or STING agonists DMXAA/ADU-S100 for a total of 2–4 doses every 2–4 days (the detailed dosing schedule is indicated in the figures). For tumour rechallenge, 6×10^6 Hepa 1-6 cells were inoculated at the primary tumour site on day 365 in cases in which the original tumour had been cleared by previous UDSP-Hep administration, and tumour growth was monitored according to established protocols.

For cytokine-blocking experiments, neutralizing antibodies targeting CXCR3 or CCL2 were administered intraperitoneally into tumour-bearing mice at the dose of 10 mg per kg, with a 2-h lead time preceding PBS, UDSP-Hep, R848 or DMXAA administration. PTx (400 ng per mouse) was administered intraperitoneally 1 day before PBS or UDSP-Hep treatment. To deplete specific immune cell types, tumour-bearing mice were subjected to intraperitoneal treatment with isotype control, anti-CD4, anti-CD8α or anti-NK1.1 at a dose of 5 mg per kg 2 days before UDSP-Hep administration. Macrophage depletion was done by using Clophosome (FormuMax, F70101C-NC) or anti-CSF1R. For the former, tumour-bearing mice received intravenous injections of 120 μl of clodronate liposomes 24 h before treatment with UDSP-Hep. For CSF1R blockade, 300 μg of anti-CSF1R was administered intraperitoneally every 3 days, initiated 72 h before the first UDSP-Hep injection. The efficiency of cell depletion was verified by flow cytometry analysis.

The lymphadenectomy procedure was performed as previous described[39]. Before the surgery, B16F10-OVA tumours were implanted subcutaneously into the hind flank. Bilateral inguinal lymphadenectomy was performed on day 9 after tumour challenge. Post-operation mice were intratumourally injected with PBS or UDSP-Hep on days 12, 14 and 16 after tumour challenge.

Mouse serum cytokine analysis

The indicated amounts of ADP-Hep or UDPS-Hep in 100 μl of PBS were injected intraperitoneally, subcutaneously, intramuscularly or intravenously into 8-week-old C57BL/6, 129 or BALB/c mice. Blood was collected after a 12 h interval and subsequently centrifuged for serum isolation. To compare different compounds, indicated amount of UDSP-Hep, R848, or ADU-S100 in 100 μl PBS was injected intravenously into C57BL/6 mice and mouse serum was collected 4 h after administration. Cytokine concentrations in the serum were measured using ProcartaPlex multiplex immunoassay (eBioscience). The heat map of cytokine concentration across samples was generated using the pheatmap (v.1.0.12) package in R.

Mouse immunizations and anti-OVA measurement

Wild-type or *Alpk1*$^{-/-}$ C57BL/6, BALB/c or 129 mice were immunized intramuscularly on day 0 and day 7 with 100 μg of OVA (Sigma-Aldrich, A5503) alone or together with different adjuvants. To compare different strains, an additional immunization was administered on day 14. Then, 7 days after the last immunization, mice were euthanized, and sera were collected by centrifugation of the whole blood at 1,200*g* for 15 min. To measure anti-OVA production, 96-well microtitre plates (Nunc) were coated with 5 μg ml^{-1} OVA in carbonate buffer (pH 9.6) and incubated for 2 h at 37 °C. The plates were washed with PBST (PBS containing 0.05% Tween-20) and blocked with 2% BSA in PBST overnight at 4 °C. After another round of washing, 100 μl of appropriately diluted sera were added into one well in triplicates, followed by incubation for 2 h at 37 °C. The plates were then washed with PBST again and incubated with HRP-labelled goat anti-mouse IgG (1:6,000, Cytiva) for 1 h at 37 °C. Ortho-phenylenediamine (0.4 mg ml^{-1}, Sigma-Aldrich) and H_2O_2 (1 μl ml^{-1}) in phosphate citrate buffer (0.15 M, pH 5.0, 100 μl per well) were added; the plates were incubated for 15 min at room temperature. The reaction was terminated by adding 50 μl of 2 M H_2SO_4 into each well. The optical density was immediately measured at 490 nm using an ELISA plate reader (TECAN).

Stability analysis of ADP-Hep and its analogues by LC–MS/MS

250 μg ml^{-1} ADP-Hep, UDP-Hep, ADSP-Hep or UDSP-Hep (50 μl) were incubated in PBS or 20% FBS/PBS (v/v) at 30 °C for 0 min, 10 min, 30 min, 1 h, 2 h, 3 h, 5 h or 8 h. Then, 200 μl of methanol was added; the samples were vortex-mixed and centrifuged at 13,000*g* for 15 min at 4 °C. Standard solutions of ADP-Hep, UDP-Hep, ADSP-Hep and UDSP-Hep at 1 mM were serially diluted in 1:1 methanol/H_2O (v/v) to prepare working solutions of 2, 5, 10, 20, 50 and 100 μM.

LC–MS/MS was performed on a Thermo Vanquish UHPLC equipped to a Thermo Q Exactive HF-X mass spectrometer. A Merck ZIC-HILIC column (2.1 × 100 mm, 3.5 μm) was used for separation; the injection volume was 5 μl. The mobile phases were 10 mM ammonium acetate in 5% acetonitrile (ACN)/water (A) and 10 mM ammonium acetate in 95% ACN/water (B). The following gradient was applied: 0–5 min, 99% B; 5–20 min, 99–20% B; 20–21 min, 20–99% B; 21–25 min, 99% B. The flow rate was 0.5 ml min^{-1}; the column temperature was 40 °C. Full-scan mass spectra were acquired in the range of *m*/*z* 66.7 to 1,000 with the following ESI source settings: spray voltage, 2.5 kV; auxiliary gas heater temperature: 380 °C, capillary temperature, 320 °C; sheath gas flow rate, 30 units; auxiliary gas flow, 10 units in the negative mode. MS1 scan parameters included resolution 60,000, AGC target 3e6, and maximum injection time 200 ms. Data processing was performed using Thermo Xcalibur software (v.4.2).

LC–MS/MS analysis of UDSP-Hep in tumours, tdLNs and plasma

For PK analysis, UDSP-Hep (2.5 mg per kg, 100 μl in PBS) was reconstituted and administered intravenously or subcutaneously into 8-week-old female C57BL/6 mice. Blood samples were collected in K_2EDTA anticoagulant tubes at pre-dose and 5 min, 15 min, 30 min, 1 h, 2 h, 4 h, 7 h, and 24 h post-dose timepoints. Plasma was isolated by centrifugation at 3,000*g* for 7 min at 4 °C. Then, 20 μl of plasma was mixed with 4 μl of water and 200 μl of ice-cold ACN/methanol (1:1, v/v) containing 1 μM ginsenoside Rb1 (as an internal standard). After vortex-mixing, the samples were centrifuged at 4,000 rpm for 15 min at 4 °C. To measure tissue distribution, B16F10-OVA tumour-bearing mice were peritumourally injected with UDSP-Hep (2.5 mg per kg, 100 μl in PBS). Then, 15 min after the injection, mice were deeply anaesthetized by CO_2 asphyxiation and systemically perfused with 20 ml saline. Tumours and tdLNs were collected, rinsed five times with ice-cold saline and blotted dry. Tissues were homogenized (w/v, 1:9) in ice-cold ACN/15 mM PBS (v/v, 1:2). Then, 1 ml of homogenates was added into 4 ml precipitant (ACN/MeOH, v/v, 1:1, with 1 μM Rb1), vortexed and centrifuged at 4,000 rpm for 15 min. The supernatants were twofold diluted with water before LC–MS/MS analysis.

The desired concentrations of working solutions were achieved by diluting stock solution of analyte with water. Then, 4 μl of working solutions were added to 20 μl of the blank female C57BL/6 mouse plasma to prepare calibration standards of 2–2,000 ng ml^{-1} (2, 4, 10, 20, 40, 100, 400, 1,000 and 2,000 ng ml^{-1}) in a total volume of 24 μl. Then, 5 μl of working solutions were added to 50 μl of the blank female C57BL/6N mice tumour homogenates or tdLN homogenates to obtain calibration standards of 1–2,000 ng ml^{-1} (1, 2, 5, 10, 20, 50, 100, 500, 1,000 and 2,000 ng ml^{-1}) in a total volume of 55 μl.

LC–MS/MS analysis was performed on the TRIPLE QUAD 6500+ system. A Waters ACQUITY UPLC BEH Amide column (2.1 × 50 mm, 1.7 μm) was used for separation. The injection volume was 5 μl. The mobile phases consisted of 5 mM ammonium acetate in water (A) and ACN (B). For plasma samples, the following gradient was applied: 0–0.3 min, 95% B; 0.3–1.5 min, 95–38% B; 2.5–2.51 min, 38–95% B, 2.51–3.00 min, 95% B. For tumour and tdLN samples, the following gradient was applied: 0–0.3 min, 98% B; 0.5–2.0 min, 80–50% B; 2.5–2.51 min, 50–98% B; 2.51–3.00 min, 98% B. The flow rate was 0.8 ml min^{-1}, and the column temperature was 25 °C. Multiple-reaction monitoring was acquired with the following ESI source settings: ion spray voltage: −4,500 V; temperature: 650 °C; ion source gas 1, 50 psi; ion source gas 2, 50 psi; curtain gas, 30 psi; collision gas, 9. *m*/*z*: 610.95/338.80. Data processing was performed with Analyst Software v.1.7.2.

Semi-quantitative PCR

THP-1 cells were differentiated with 50 nM phorbol 12-myristate 13-acetate (PMA) for 48 h. The differentiated or native THP-1 cells were then stimulated with ADP-Hep, UDP-Hep, UDSP-Hep, R848 or ADU-S100 for 4 h or 12 h, while RPMI-8226 cells were stimulated the agonists for 4 h. RNAs were extracted using the FastPure Cell/Tissue Total RNA Isolation Kit (Vazyme, RC101-01). Primary BMDMs were seeded into a six-well plate at a density of 1.5 × 10^5 cells per well. After allowing to adhere for 2 h, cells were treated with varying concentrations of ADP-Hep, UDP-Hep, UDSP-Hep, R848 or ADU-S100 and continuously cultured for 4 h, 6 h or 12 h as indicated. RNA extraction from BMDMs was carried out using the RNeasy Plus Micro Kit (QIAGEN, 74034). For PCR analyses, 1 μg of purified RNAs was reverse-transcribed into cDNA using the ABScript III RT Master Mix for qPCR with gDNA Remover (ABclonal, RK20429). The cDNA samples were appropriately diluted and used for quantitative PCR (qPCR) analysis. PCR amplification and detection were performed using SYBR Premix Ex Taq (Tli RNase H Plus, TAKARA). The following primers were used: 5′-GGTGAGAAGAGATGTCTGAATCC-3′ (forward, F) and 5′-GTCCATCCTTGGAAGCACTGCA-3′ (reverse, R) for human *CXCL10*, 5′-AAACAGATGAAGTGCTCCTTCCAGG-3′ (F) and 5′-TGGAGAACACCACTTGTTGCTCCA-3′ (R) for human *IL1B*, 5′-AATCTGGCAACCCTAGTCTGCTA-3′ (F) and 5′-AAACCAAGGCACAGTGGAACA-3′ (R) for human *CXCL8*, 5′-AGAATCACCAGCAGCAAGTGTCC-3′ (F) and 5′-TCCTGAACCCACTTCTGCTTGG-3′ (R) for human *CCL2*, 5′-CTCTTCTGCCTGCTGCACTTTG-3′ (F) and 5′-ATGGGCTACAGGCTTGTCACTC-3′ (R) for human *TNF*, 5′-TGAAAAGTTTAAAAACAATCCACAA-3′ (F) and 5′-GCAAATGGTGGTCAAACTCC-3′ (R) for human *ALPK1*, 5′-CTTGGATTCCTACAAAGAAGCAGC-3′ (F) and 5′-TCCTCCTTCTGGAACTGCTGCA-3′ (R) for human *IFNB1*, 5′-GCCTTGCTGAAGTGTGGAGGAA-3′ (F) and 5′-ATCCAGGCGATAGGCAGAGATC-3′ (R) for human *IFIT1*, 5′-CCAAGTGCTGCCGTCATTTTC-3′ (F) and 5′-GGCTCGCAGGGATGATTTCAA-3′ (R) for mouse *Cxcl10*, 5′-CCCTCACACTCAGATCATCTTCT-3′ (F) and 5′-GCTACGACGTGGGCTACAG-3′ (R) for mouse *Tnf*, 5′-AAGATCAAGGCATCTGGGAAAG-3′ (F) and 5′-CCTCTGGGAATGTTCTGGTTC-3′ (R) for mouse *Ifi205*, 5′-TCCAGAGCTTGAAGGTGTTGCC-3′ (F) and 5′-AACCAAGGGAGCTTCAGGGTCA-3′ (R) for mouse *Cxcl1*, 5′-CATCCAGAGCTTGAGTGTGACG-3′ (F) and 5′-GGCTTCAGGGTCAAGGCAAACT-3′ (R) for mouse *Cxcl2*, 5′-TGGACATTGCTACCACAGAGGC-3′ (F) and 5′-TTGCCTTCAGCACCTCTGTCCA-3′ (R) for mouse *Mx1*,

5′-GCCTTTGCCATCCAAGAGATGC-3′ (F) and 5′-ACACTGTCTGCTGGTGG AGTTC-3′ (R) for mouse *Ifnb1*, 5′-AGGTCGGTGTGAACGGATTTG-3′ (F) and 5′-TGTAGACCATGTAGTTGAGGTCA-3′ (R) for mouse *Gapdh*, and 5′-GTCTCCTCTGACTTCAACAGCG-3′ (F) and 5′-ACCACCCTGTTGCTGT AGCCAA-3′ (R) for human *GAPDH*. Gene expression was normalized using the $\Delta\Delta C_t$ method and presented as fold changes.

Human PBMCs

Human PBMCs, obtained from SAILYBIO (Sailybio Tech) or MILECELL (MileCell Biotechnology), were rapidly thawed in a 37 °C water bath. After centrifugation, cells were resuspended in TCM and cultured in a 10-cm dish for 6 h at 37 °C in a 5% CO_2 incubator. The cells were then seeded in a 96-well plate at a density of 3×10^5 cells per well and treated with ADP-Hep, UDSP-Hep, TLR7 agonist (Compound 41c-A) or ADU-S100 for 12 h. Cytokines in cell supernatants were measured using LegendPlex COVID-19 Cytokine Storm Panel 1 (BioLegend). Data were acquired on a BD Celesta flow cytometer with HTS mode and analysed using LegendPlex Data Analysis Software Suite.

Intratumour cytokine analysis

To measure intratumoural cytokines, mice were implanted subcutaneously with B16F10-OVA or Hepa1-6 tumours. After reaching the desired tumour sizes, UDSP-Hep (2.5 mg ml^{-1}) was intratumourally administered. Isolation of TIFs was conducted using an established protocol with slight modifications[47]. In brief, bulk tumour tissues were placed onto a 40-μm cell strainer and centrifuged at 40*g* for 5 min at 4 °C to eliminate the surface liquid. The tumours were diced and centrifuged at 400*g* for 10 m at 4 °C; the fluid obtained was collected as TIFs. The TIFs were centrifuged at 10,000*g* for 5 m to eliminate insoluble particles and cytokines in the TIFs were quantified using the LegendPlex MU Anti-virus response panel (BioLegend, 740621) according to the manufacturer's instructions.

scRNA-seq analysis

Mice bearing B16F10-OVA tumours were administered with PBS or UDSP-Hep on days 10, 12, 14 and 16. On day 19, three tumours from each experimental group were excised and enzymatically digested as described below. Cells were then stained with PE-anti-mouse CD45. For tumour-infiltrating immune cells analysis, the $CD45^+$ population was sorted using a BD FACSAria Fusion flow cytometer. For the whole-tumour cell component profiling, $CD45^+$ and $CD45^-$ cells were separately collected and reconstituted at a 3:2 ratio. Cell viability was real-time monitored during the preparation of the cell suspension. In total, 10,000 cells (around 1,000 single cells per μl) from each experimental group were barcoded and pooled using the 10x Genomics device. Sample preparation was carried out in accordance with the manufacturer's protocol, and sequencing was performed on an Illumina NextSeq sequencer.

The sequencing data were imported into Cell Ranger (v.7.0.0) for sample demultiplexing, barcode processing, alignment, filtering and UMI counting. In the first step of quality control, cells sequenced with <300 genes or >6,000 genes were removed, and cells with greater than 10% of sequenced genes being mitochondrial genes were subsequently excluded. Genes expressed in fewer than three cells across each sample were also excluded. scDblFinder (v.1.16.0) was used to detect and remove possible multiple cells captured within the same droplet (also called doublets/multiplets). A total of 12,984 sequenced cells were obtained after the quality control step. Subsequent data processing and analyses were performed in Seurat (v.5.0.0). The gene counts were subjected to library size normalization using Seurat function NormalizeData. Principal component analysis (PCA) and nearest-neighbour graphs were computed to visualize the data on a UMAP projection. Subsequently, Harmony batch correction was applied to rectify PCA embeddings to mitigate technical batch effects across experiments. Cells were clustered into 19 distinct populations using the Louvain algorithm. Differentially expressed genes were identified using Seurat function FindAllMarkers and used to define the identity of each population. For in-depth analysis of T cell or macrophage subtypes, *Cd3e* and *Cd3d* double-positive T cells and *Cd68*-expressing macrophages were extracted for new PCA embeddings, nearest-neighbourh graphs and harmony batch corrections. The paired quantile–quantile plot was calculated using the Wilcoxon rank-sum two-sided test between the two treatment conditions. The VlnPlot function from the Seurat (v.5.0.0) package was used to generate violin plots for *Alpk1* and *Tifa*. This analysis was performed on a subset of the data containing only cells from the untreated group. In these plots, the distribution of normalized expression is shown for each cell type, with individual dots overlaid to represent single cells.

Flow cytometry analyses of immune cells

In tumour-control efficacy assays, B16F10-OVA or MC38 tumour-bearing mice were peritumourally injected with UDSP-Hep or PBS on days 8, 10, 12 and 16, with tumours and tdLNs collected on day 17 for analysis. To compare different agonists, B16F10-OVA tumours were treated with a single 50-μg dose of UDSP-Hep, DMXAA or their combination on day 8, followed by tdLNs collection on day 11. To evaluate T cell memory responses, Hepa1-6 tumour-bearing mice were administered with 50 μg of UDSP-Hep, DMXAA or PBS on days 8, 11 and 14; skin (tumour site), tdLNs, spleen and non-tumour dLNs were collected at days 23 and 60.

tdLNs (ipsilateral axillary, brachial and inguinal lymph nodes) were excised, minced and enzymatically digested in RPMI 1640 containing 0.5 mg ml^{-1} collagenase D (Roche, COLLD-RO) and 0.1 mg ml^{-1} DNase I (Sigma-Aldrich, DN25) at 37 °C for 30 min. Tumour tissues were weighed and dissociated using the mouse Tumour Dissociation kit (Miltenyi) in a MACS Dissociator (Miltenyi, program m-TDK-1), and filtered through 70-μm strainers. Skin samples were digested with 150 U ml^{-1} collagenase II (Diamond, A004174) and 0.02 mg ml^{-1} DNase I, while spleens were mechanically dissociated through a 70-μm mesh. Red blood cells were lysed in the ACK buffer (150 mM ammonium chloride, 10 mM potassium bicarbonate and 0.1 mM disodium EDTA, pH 7.4). For scRNA-seq, tumour–immune cell mixtures were directly stained. For T cell analysis, lymphocytes were enriched by discontinuous Percoll (Cytiva, 17089101) gradient centrifugation (44%/67%). After appropriate washing, cells were stained with LIVE/DEAD Fixable Near-IR Dead Cell Stain Kit (Invitrogen, L34975) and blocked with anti-mouse CD16/32. Cells were further stained with antibodies for specific surface markers in the MACS buffer (2% FBS and 2 mM EDTA in PBS) for 45 min on ice. After the staining, cells were washed twice with the MACS buffer and fixed using the Foxp3/Transcription Factor Staining Buffer Set (eBiosciences, 00-5523-00).

For tetramer staining, APC-labelled tetramers were added to the cell suspension and stained for 1 h on ice before surface marker staining. To assess cytokine and transcription factor expression, immune cells were restimulated with Leukocyte Activation Cocktail Supplemented with BD GolgiPlug (BD Pharmingen, 550583) for 4 h. Cells were then collected, washed with the MACS buffer and stained for surface markers as above described. After fixation and washing, cells were stained with antibodies for specific cytokine and transcription factors. The stained samples were analysed on the BD FACSAria III or BD LSRFortessa flow cytometer. The flow cytometry data were processed and analysed using FlowJo software.

Bone marrow chimera

Lethally irradiated recipient mice were subjected to whole-body irradiation (twice with 5.5 Gy with a 4 h interval). Then, 5×10^6 bone marrow cells, isolated from wild-type and *Alpk1*$^{-/-}$ donor mice, were transplanted intravenously 4 h after irradiation. Cells were collected by flushing femurs/tibias with cold PBS, lysed in the ACK buffer and filtered through 40-μm strainers. The recipients were maintained with antibiotic water for 14 days after the transplantation. Peripheral blood

chimerism was assessed at week 8 by flow cytometry using anti-CD45.1. On week 9, B16F10-OVA cells were grafted subcutaneously, and PBS or UDSP-Hep (50 μg per mouse) was administered when the tumour volume reached 100 mm^3.

Cell sorting and adoptive cell transfer

Naive $CD45.1^+$ OT-I $CD8^+$ T cells were isolated by flow cytometry sorting for live $CD8^+CD62L^+CD44^-$ populations 2×10^5 cells were adoptively transferred intravenously into $CD45.2^+$ mice bearing established B16F10-OVA tumours (day 9 after implantation). Recipient mice were injected with cyclophosphamide (4 mg per mouse, intraperitoneal injection) 20 h before T cell transfer. On day 10, PBS or UDSP-Hep (100 μg) was administered intratumourally. On day 22, $CD45.1^+CD8^+CD44^+$ OT-I T cells were isolated from tdLNs and 8×10^4 cells were injected intravenously into *Cd8a*$^{-/-}$ mice bearing B16F10-OVA tumours. Tumour volumes were monitored every 3 days.

B16F10-OVA antigen-presentation assay

B16F10-OVA cells were treated with UDSP-Hep or ADU-S100 in the presence or absence of 1 ng ml^{-1} IFNγ (Novoprotein, C746) for 48 h. Cells were washed with the MACS buffer and stained with the LIVE/DEAD Fixable Near-IR Dead Cell Stain Kit to mark the dead cells. The cells were then stained with anti-H-$2K^b$ bound to SIINFEKL antibody and analysed on a BD FACSCelesta flow cytometer with HTS mode (BD Biosciences). The data were analysed using the FlowJo software.

In vitro BMDM and iCD103-DC activation and OT-I $CD8^+$ T cell priming assay

Primary iCD103-DCs were generated as previously described[48]. In brief, bone marrow cells collected from wild-type and *Alpk1*$^{-/-}$ mice were cultured in 10-cm dishes at a density of 1×10^6 cells per ml in TCM. For iCD103-DC differentiation, cells were treated with 200 ng ml^{-1} recombinant mouse Flt3L (ABclonal, RP01058) and 2 ng ml^{-1} mouse GM-CSF (Peprotech, 315-03). Parallel BMDM differentiation cultures were supplemented with 50 ng ml^{-1} recombinant mouse M-CSF (Novoprotein, CB34). Medium was half-changed every 3 days; BMDMs and iCD103-DCs were collected on days 7 and 16, respectively, for subsequent analyses.

iCD103-DCs or BMDMs were seeded in a 96-well plate at a density of 2×10^5 cells per well and stimulated with LPS or ADP-Hep, UDSP-Hep, R848 or ADU-S100 for 8 h. After the stimulation, cells were blocked with anti-mouse CD16/32 and then stained with fluorochrome-conjugated antibodies against anti-mouse CD11c, I-A/I-E, CD40, CD80, and CD86 for iCD103-DCs and CD11b, F4/80, and CD86 for BMDMs. The stained cells were analysed on the BD LSRFortessa flow cytometer.

For $CD8^+$ T cell priming assay, well-differentiated iCD103-DCs or BMDMs were seeded in a 96-well plate at a density of 1×10^5 cells per well and stimulated with LPS, ADP-Hep, UDSP-Hep or ADU-S100 combined with 1 μg ml^{-1} OVA for 8 h. OT-I T cells were prepared from mouse spleen and mesenteric lymph nodes, and lymphocytes were enriched using lymphocyte separation solution (DAKEWE, 7211011). $CD3^+$ T cells were further enriched using the MojoSort mouse $CD3^+$ T cell isolation kit (BioLegend, 480024). The T cells were counted and labelled with carboxyfluorescein succinimidyl ester (CFSE) (Tonbo, 13-0850-U500). Labelled T cells (2×10^5 cells per well) were co-cultured with stimulated iCD103-DCs or BMDMs for 96 h or 72 h, respectively. Cells were then stained with anti-mouse CD8α and DAPI for dead cell exclusion before flow cytometry analysis.

For tumour control experiment, well-differentiated iCD103-DCs were primed with 1 μg ml^{-1} OVA alone or combined with 100 nM UDSP-Hep or ADU-S100 for 8 h. After washing with PBS, 5×10^5 cells were s.c. injected proximal to tdLNs in B16F10-OVA tumour-bearing mice on days 7, 10 and 13.

Statistics and reproducibility

Statistical analyses were conducted using GraphPad Prism (v.10) and *P* values determined accordingly. Two-tailed unpaired Student's *t*-tests, Welch's *t*-tests, one-way ANOVA and two-way ANOVA were used for intergroup comparisons as noted in the legends unless indicated otherwise. Compound dose–response curves were delineated using a three-parameter logistic-nonlinear regression model, enabling the calculation of EC_{50} values. Two-way ANOVA and log-rank (Mantel–Cox) test were used for statistical comparisons of tumour volume and mouse survival data, respectively. Two-tailed Wilcoxon rank-sum tests were applied for differential expression or activity score analysis of scRNA-seq data. No statistical methods were used to predetermine sample sizes for mouse experiments; generally, a minimum of five mice was assayed in each group. While the assumption of normal data distribution was made, formal testing was not executed. Animals were randomized before treatments, and data collection and analysis were conducted without blinding to the experimental conditions. Information concerning reproducibility for the experiments shown in this study is given in the figure legends of the corresponding data.

Reporting summary

Further information on research design is available in the Nature Portfolio Reporting Summary linked to this article.

Data availability

The scRNA-seq datasets generated in this study are available under GEO accession numbers GSM8479167 and GSM8479168. Raw RNA-seq datasets are available under GEO accession numbers GSE308610 and GSE308482. All other data supporting the findings of this study are provided with the Article and its Supplementary Information. Source data are provided with this paper.

46. Zhao, Y. et al. The NLRC4 inflammasome receptors for bacterial flagellin and type III secretion apparatus. *Nature* **477**, 596–600 (2011).
47. Wiig, H., Tenstad, O., Iversen, P. O., Kalluri, R. & Bjerkvig, R. Interstitial fluid: the overlooked component of the tumor microenvironment? *Fibrogenesis Tissue Repair* **3**, 12 (2010).
48. Mayer, C. T. et al. Selective and efficient generation of functional Batf3-dependent $CD103^+$ dendritic cells from mouse bone marrow. *Blood* **124**, 3081–3091 (2014).

Acknowledgements We thank X. Zhang for providing MB49 cells; X. Xia for *Batf3*$^{-/-}$ mice; Z. Shen at BeiGene for MC38 cells and anti-PD-1; the staff at Pyrotech for Hepa 1-6 cells and *ALPK1*-humanized mice; F. Du at Adagene for anti-CTLA-4, anti-4-1BB and anti-PD-L1; L. Gao and L. Ye for assistance with immunological assays; Y. Xu and the members of the NIBS Laboratory Animal Resource Center for mouse breeding; the staff at the NIBS sequencing centre for RNA-seq experiments; the staff at the CIBR Laboratory Animal Resource Center for animal radiation; and W. Shi and Y. Wang for technical assistance. The work was supported by the Basic Science Center Project (82388201) of the National Natural Science Foundation of China (NSFC), the Strategic Priority Research Program of Chinese Academy of Sciences (XDB37030202 and XDB29020202), the National Key Research and Development Program of China (2022YFA1304700) and the Chinese Academy of Medical Sciences Innovation Fund for Medical Sciences (2019-I2M-5-084) to F.S. F.S. is also supported by the Tencent New Cornerstone Investigator Program.

Author contributions J.L., X.T. and F.S. conceived the study. J.L. and X.T. performed the experiments. Y. Li synthesized ADP-Hep and it analogues, supervised by C.L.; Y. Luo analysed the scRNA-seq data. Y.M. helped with the LC–MS analyses. Y.W., H.H., Y.S. and J.D. provided technical assistance and valuable suggestions. P.Z. was involved in the early stage of the study and made some initial observations. J.L., X.T. and F.S. analysed the data and wrote the manuscript with input from all of the authors. All of the authors discussed the results and commented on the manuscript.

Competing interests F.S. is the scientific founder and chair of the scientific advisory board of Pyrotech Therapeutics. This relationship did not influence this study. The other authors declare no competing interests.

Additional information

Supplementary information The online version contains supplementary material available at https://doi.org/10.1038/s41586-025-09828-9.

Correspondence and requests for materials should be addressed to Feng Shao.

Peer review information *Nature* thanks Matteo Iannacone and the other, anonymous, reviewer(s) for their contribution to the peer review of this work.

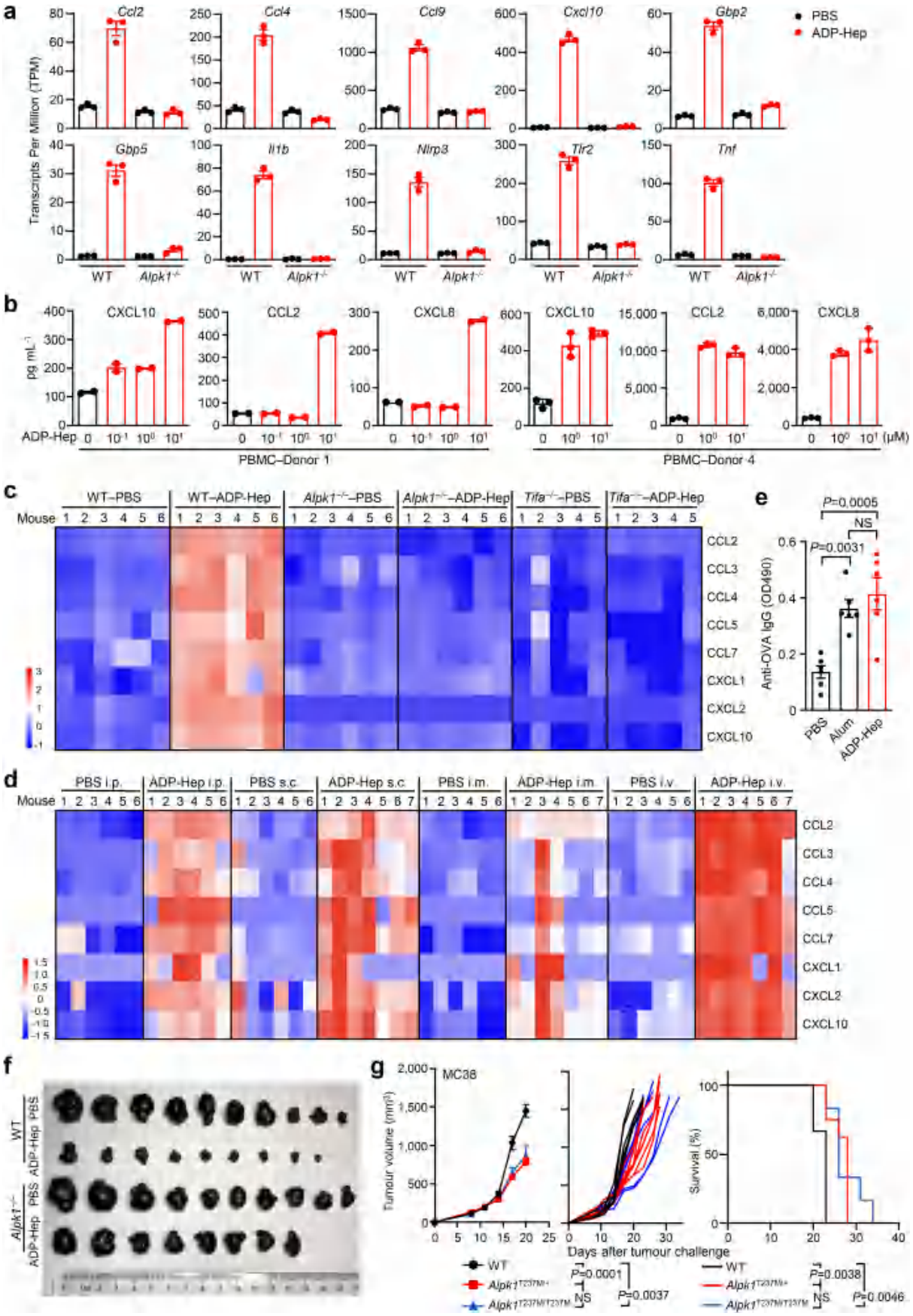

Extended Data Fig. 1 | See next page for caption.

Extended Data Fig. 1 | Activation of ALPK1 by ADP-Hep stimulates innate and adaptive immune responses as well as antitumour immunity. a, BMDMs from WT or *Alpk1*$^{-/-}$ C57BL/6 mice were treated with PBS or 100 μM ADP-Hep for 4 h. Transcript levels of the indicated genes are shown (mean ± s.e.m., $n = 3$). **b**, Cytokine concentrations in the supernatants of ADP-Hep-treated human PBMCs (mean ± s.d.); see Fig. 2d and Supplementary Fig. 1b for more comprehensive data. **c**, Heatmap of cytokine concentrations in the sera of WT ($n = 6$), *Alpk1*$^{-/-}$ ($n = 6$), or *Tifa*$^{-/-}$ ($n = 5$) C57BL/6 mice injected (i.v.) with PBS or ADP-Hep (500 μg per mouse). **d**, Heatmap of cytokine concentrations in the sera of C57BL/6 mice injected with PBS ($n = 6$) or ADP-Hep (500 μg per mouse; $n = 6$ for i.p. and 7 for the other groups) intraperitoneally (i.p.), subcutaneously (s.c.), intramuscularly (i.m.), or intravenously (i.v.). **e**, WT C57BL/6 mice were immunized with OVA (100 μg per mouse) alone or in combination with aluminium (Alum, 2 mg per mouse) or ADP-Hep (500 μg per mouse). Anti-OVA IgG production was measured by ELISA on day 14 after immunization, and the absorbance values are shown as mean ± s.e.m. ($n = 6$); *P* values were calculated using one-way ANOVA. **f**, WT or *Alpk1*$^{-/-}$ C57BL/6 mice bearing B16F10-OVA tumours were treated with PBS or ADP-Hep (500 μg per mouse) ($n = 8$–10 mice as shown in the tumour photographs taken on day 22 after tumour challenge). **g**, MC38 tumours were grafted (s.c.) into WT ($n = 6$), *Alpk1*$^{T237M/+}$ ($n = 8$), or *Alpk1*$^{T237M/T237M}$ ($n = 6$) C57BL/6 mice. Left, average tumour growth curves for the time duration when all mice within the group remained on study (mean ± s.e.m., two-way ANOVA, NS, not significant); middle, tumour growth curves in individual animals; right, mouse survival (log-rank (Mantel–Cox) test). All data are representative of three independent experiments.

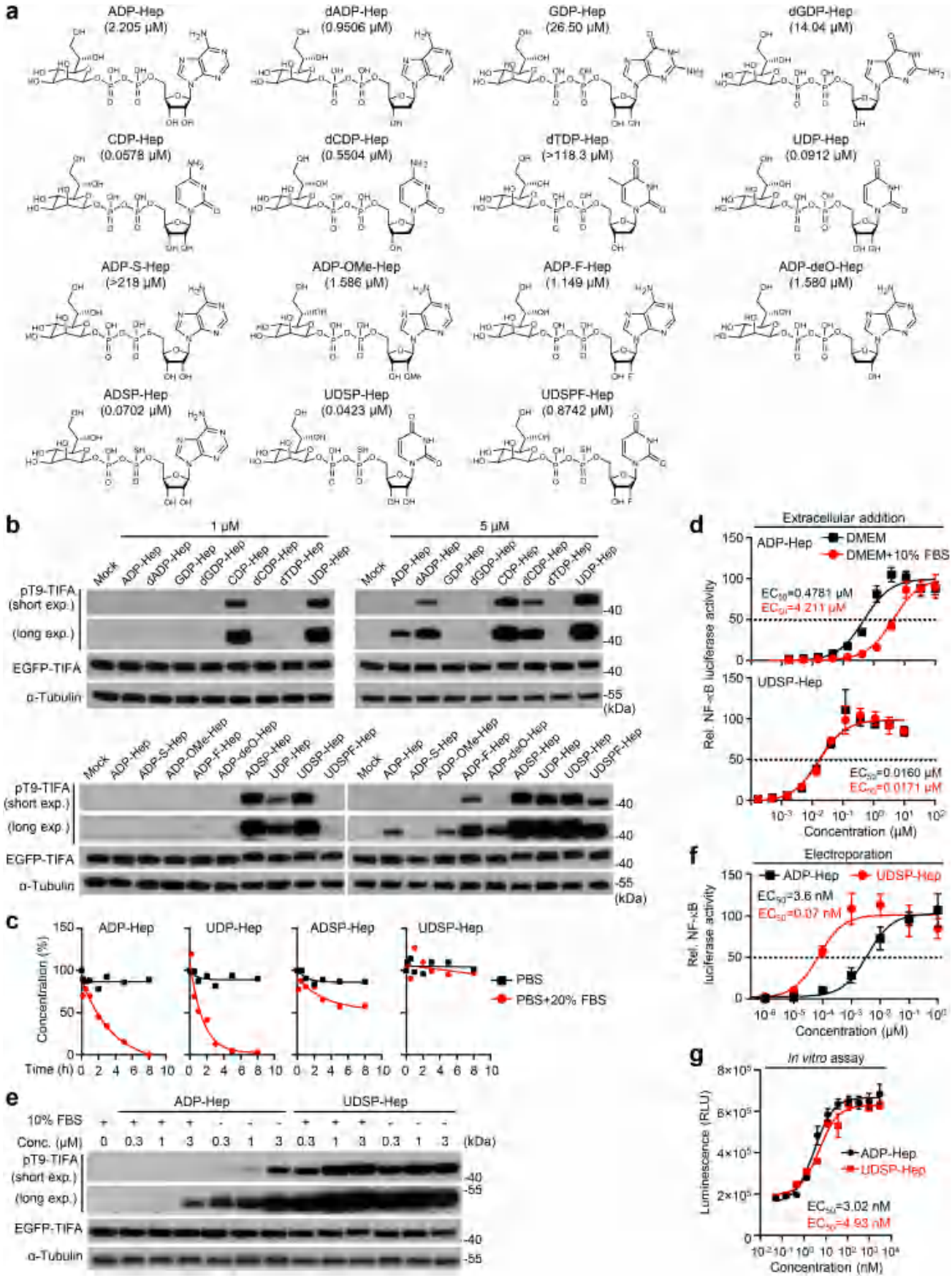

Extended Data Fig. 2 | See next page for caption.

Extended Data Fig. 2 | Chemical modifications of ADP-Hep identifies UDSP-Hep as a more potent and stable ALPK1 agonist. a, Chemical structures and EC_{50} of ADP-Hep analogues. Synthesis and preparation of the analogues are in Supplementary Data 1. EC_{50} was determined using the NF-κB luciferase reporter assay in HEK293 T cells (see Supplementary Fig. 1a). The ADP-Hep and UDSP-Hep data are the same as shown in Fig. 2b. **b**, **e**, HEK293 T cells with eGFP-TIFA integrated into the genome were treated with ADP-Hep or an indicated analogue. **c**, LC-MS analysis of the stability of ADP-Hep, UDP-Hep, ADSP-Hep, and UDSP-Hep in PBS in the presence or absence of 20% FBS (v/v). **d**, HEK293 T cells, cultured in serum-free or 10% FBS-supplemented DMEM, were stimulated extracellularly with ADP-Hep ($n = 6$) or UDSP-Hep ($n = 3$). **f**, HEK293 T cells were electroporated with ADP-Hep or UDSP-Hep ($n = 3$ for each group). **g**, Activation of recombinant human ALPK1 by ADP-Hep and UDSP-Hep in vitro, quantified via the ADP-Glo™ luminescent kinase assay (mean ± s.d.). **b**, **e**, Anti-pT9-TIFA immunoblotting. **d**, **f**, NF-κB luciferase reporter assay data (mean ± s.d.). **d**, **f**, **g**, Curves were fitted to calculate EC_{50} values. All data are representative of three independent experiments.

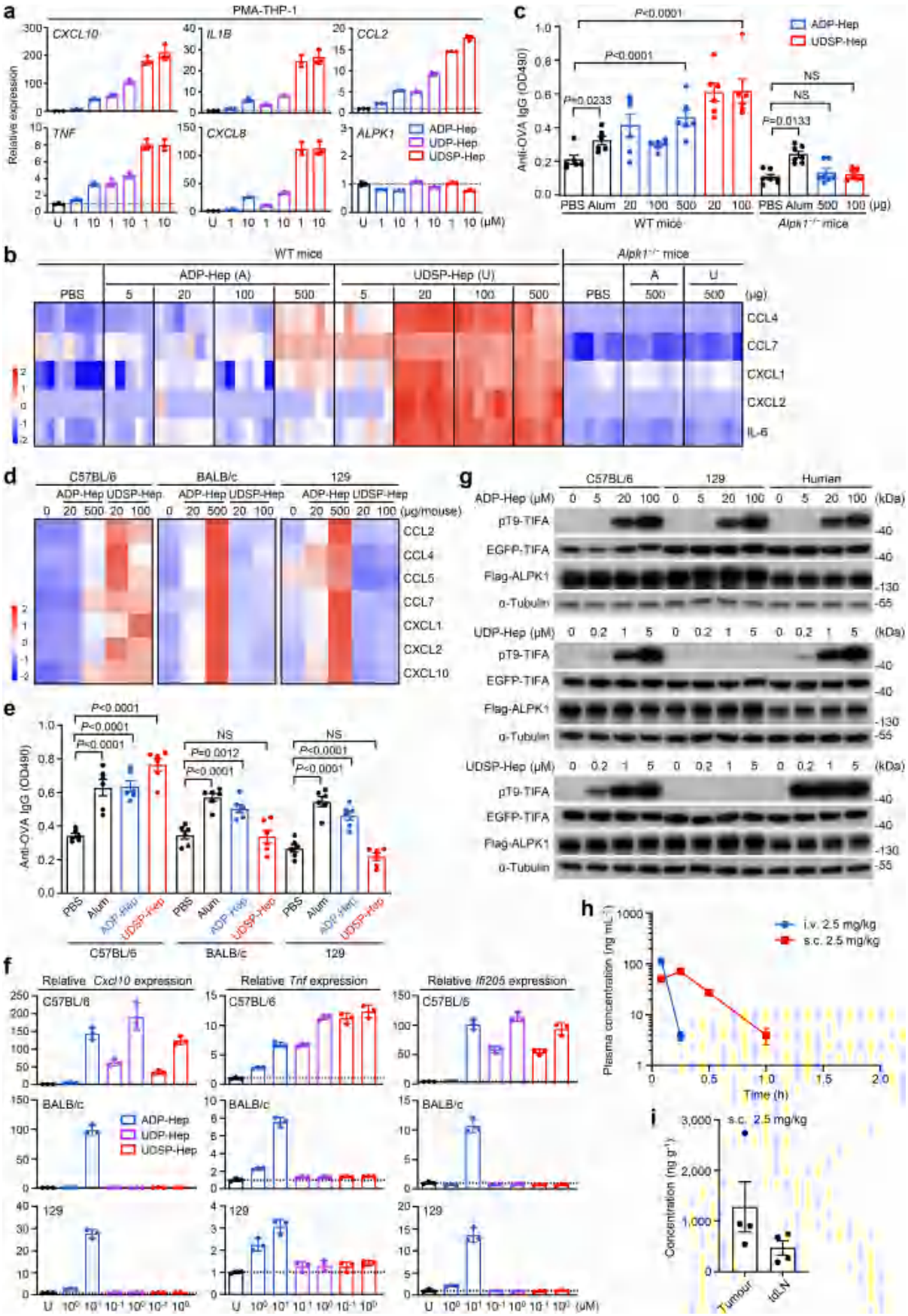

Extended Data Fig. 3 | See next page for caption.

Extended Data Fig. 3 | UDSP-Hep has much stronger immunostimulant activity than ADP-Hep and distinguishes *Alpk1* alleles in mice. a, RT-qPCR analysis of *CXCL10*, *IL1B*, *CXCL8*, *CCL2*, *TNF*, and *ALPK1* expression in PMA-differentiated THP-1 cells treated with ADP-Hep, UDP-Hep, or UDSP-Hep for 12 h. Levels of mRNA were normalized to that of *GAPDH* (mean ± s.d., $n = 3$). **b**, Heatmap of cytokine concentrations in the sera of WT or *Alpk1*$^{-/-}$ C57BL/6 mice injected (i.v.) with PBS or an indicated dose of ADP-Hep or UDSP-Hep ($n = 7$ for untreated WT group, 5 for 5-μg ADP-Hep- and 500-μg UDSP-Hep-treated WT group, and 6 for other groups). **c**, **e**, WT or *Alpk1*$^{-/-}$ C57BL/6 mice or indicated strains of mice were immunized with OVA (100 μg per mouse) alone or in combination with aluminium (Alum, 2 mg per mouse) or an indicated dose of ADP-Hep or UDSP-Hep (**c**) or ADP-Hep (500 μg per mouse), or UDSP-Hep (20 μg per mouse) (**e**). Anti-OVA IgG production was measured by ELISA on day 21 after immunization, and the absorbance values are shown as mean ± s.e.m. (**c**, $n = 6$ for WT and 7 for *Alpk1*$^{-/-}$; **e**, $n = 6$). Two-way ANOVA. **d**, Heatmap of cytokine concentrations in the sera of C57BL/6, 129, or BALB/c mice injected (i.v.) with PBS, ADP-Hep or UDSP-Hep at the indicated doses. Each lane indicates the average cytokine expression ($n = 5$–6 mice per group). **f**, RT-qPCR analyses of *Cxcl10*, *Tnf*, and *Ifi205* expression in C57BL/6, 129, or BALB/c strain-derived BMDMs treated with ADP-Hep, UDP-Hep, or UDSP-Hep for 6 h. Levels of mRNA were normalized to that of *Gapdh* (mean ± s.d., $n = 3$). **g**, *ALPK1*$^{-/-}$ HEK293 T cells expressing eGFP-TIFA and Flag-ALPK1 derived from the C57BL/6 or 129 mice or humans were treated with ADP-Hep, UDP-Hep, or UDSP-Hep. TIFA phosphorylation was assessed by anti-pT9-TIFA immunoblotting. **h**, Serum concentrations of UDSP-Hep over time after a single s.c. or i.v. injection (2.5 mg kg^{-1}) into C57BL/6 mice. Blood was collected at 0, 0.083, 0.25, 0.5, 1, 2, 4, and 7 h after the UDSP-Hep injection; its concentrations were quantified by LC-MS/MS (mean ± s.e.m., $n = 3$). **i**, Local biodistribution after peri-tumoural injection of UDSP-Hep. The concentrations of UDSP-Hep in tumour tissues and tdLNs 15 min after the injection (2.5 mg kg^{-1}) are shown (mean ± s.e.m., $n = 4$). Data are representative of two (**h**, **i**) or three (**a**–**g**) independent experiments.

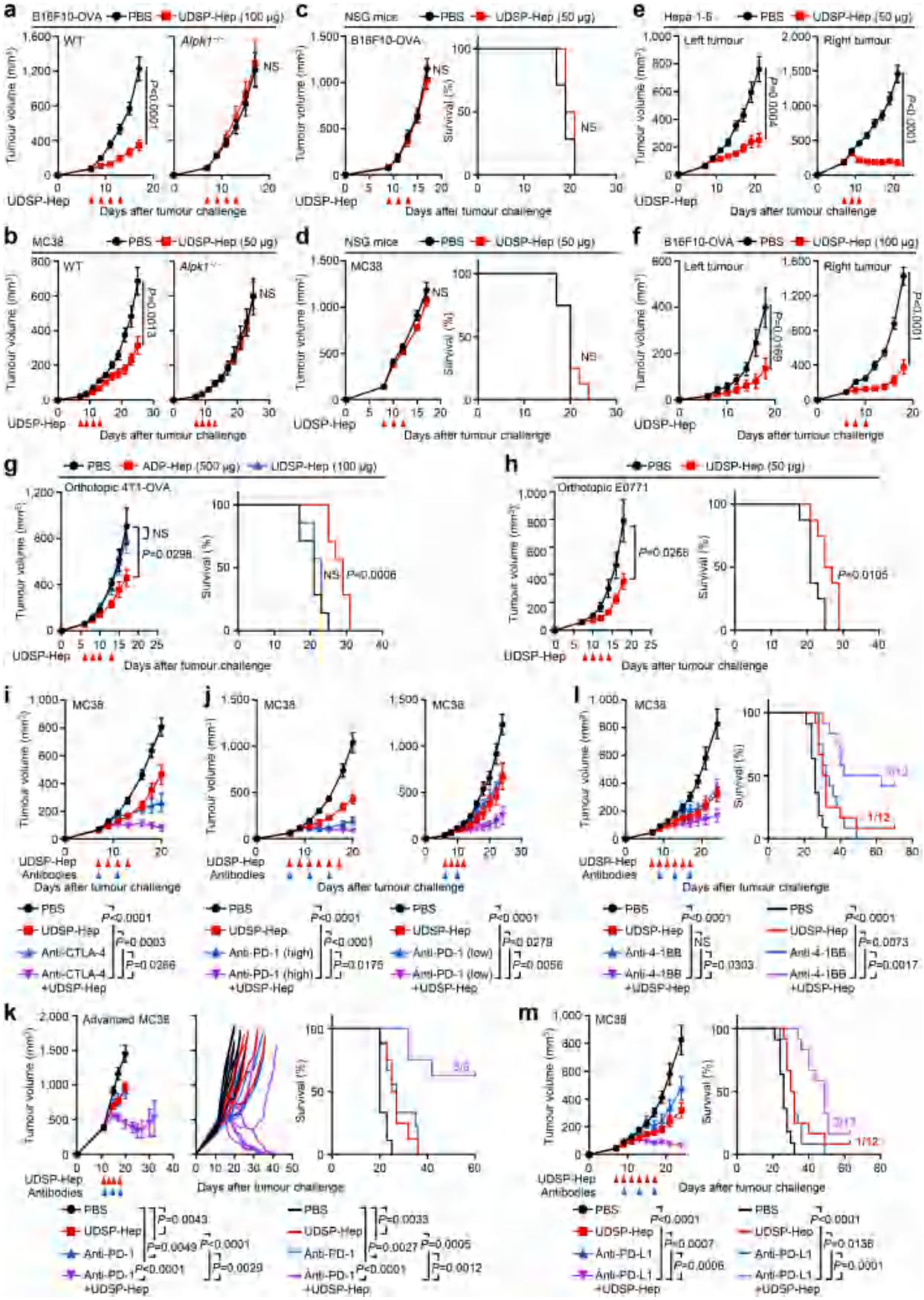

Extended Data Fig. 4 | See next page for caption.

Extended Data Fig. 4 | UDSP-Hep-induced *Alpk1*-dependent antitumour immunity in mice and can enhance the effects of various checkpoint inhibitors. a, **b**, Growth curves of B16F10-OVA (**a**) and MC38 tumours (**b**) in WT and *Alpk1*$^{-/-}$ C57BL/6 mice treated with PBS or UDSP-Hep (**a**, $n = 11$ for PBS-treated WT group and 8 for other groups; **b**, $n = 11$ for WT and 9 for *Alpk1*$^{-/-}$). **c**, **d**, Growth curves (left) and survival analysis (right) of B16F10-OVA (**c**) and MC38 tumours (**d**) treated with PBS or UDSP-Hep in NSG mice ($n = 7$ for PBS-treated B16F10-OVA and 8 for other groups). **e**, **f**, Hepa1-6 (**e**) and B16F10-OVA (**f**) were grafted into both sides of the back of C57BL/6 mice. Tumours on the right flank were treated with PBS (**e**, $n = 8$; **f**, $n = 10$) or UDSP-Hep (**e**, $n = 11$; **f**, $n = 9$). **g**, **h**, Growth curves (left) and survival analysis (right) of orthotopic 4T1-OVA (**g**) or E0771 (**h**) mammary carcinoma in BALB/c ($n = 7$) or C57BL/6 mice ($n = 8$), respectively, subjected to intratumour injection of PBS, ADP-Hep, or UDSP-Hep. **i**, **j**, Growth curves of MC38 tumours treated with PBS, UDSP-Hep (50 μg per mouse), anti-CTLA-4 antibody (0.5 mg kg^{-1}), anti-PD-1 antibody (high dose, 5 mg kg^{-1}; low dose, 0.25 mg kg^{-1}), or UDSP-Hep combined with either antibody (**i**, $n = 12$ for PBS and 11 for other groups; **j**, Left, $n = 11$ for PBS and UDSP-Hep groups, 21 for anti-PD-1, and 23 for UDSP-Hep and anti-PD-1 co-treatment group; Right, $n = 10$). **k**, Average and individual-animal tumour growth curves and mouse survival of advanced MC38 tumours (nearly 400 mm^3) treated with PBS ($n = 9$), UDSP-Hep (50 μg per mouse; $n = 8$), anti-PD-1 antibody (10 mg kg^{-1}; $n = 9$), or UDSP-Hep combined with anti-PD-1 antibody ($n = 8$). **l**, **m**, C57BL/6 mice bearing MC38 tumours were treated with PBS ($n = 11$), UDSP-Hep (50 μg per mouse; $n = 12$), anti-4-1BB antibody (5 mg kg^{-1}; $n = 12$), anti-PD-L1 antibody (5 mg kg^{-1}; $n = 12$), or UDSP-Hep combined with either antibody ($n = 12$). The PBS and UDSP-Hep-alone groups in **l** and **m** are the same experiment. **a**–**m**, Data are shown as mean ± s.e.m., and two-way ANOVA and log-rank (Mantel–Cox) tests were used for statistical comparisons of tumour volume and mouse survival data, respectively (NS, not significant). Data are representative of two independent experiments.

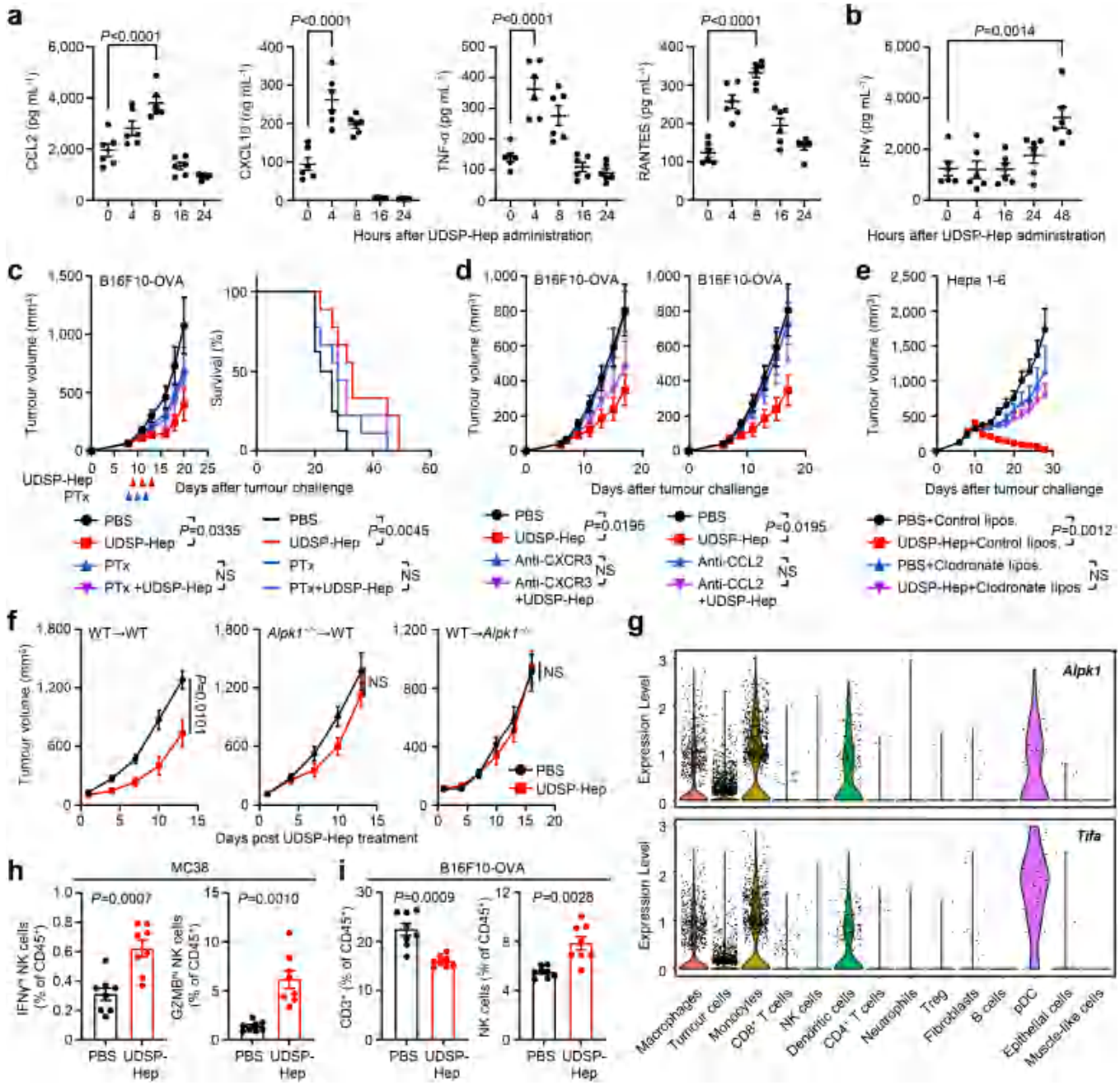

Extended Data Fig. 5 | UDSP-Hep inflames the tumours and the tumour control requires chemokines and bone marrow-derived cells.
a, **b**, Quantification of cytokines within Hepa1-6 tumours upon UDSP-Hep treatment ($n = 6$ mice per group). **c**, Growth curves (left) and mouse survival (right) of B16F10-OVA tumours treated with PBS ($n = 8$), UDSP-Hep (50 µg per mouse; $n = 9$), PTx (400 ng per mouse; $n = 9$), or UDSP-Hep combined with PTx ($n = 9$). **d**, Growth curves of B16F10-OVA tumours treated with PBS ($n = 9$), UDSP-Hep ($n = 10$), CXCR3-blocking antibody ($n = 9$), CCL2-neutralizing antibody ($n = 7$), or UDSP-Hep combined with either antibody ($n = 9$ for anti-CXCR3 plus UDSP-Hep and 7 for anti-CCL2 plus UDSP-Hep). **e**, Growth curves of Hepa1-6 tumours treated with UDSP-Hep alone or in combination with control or clodronate liposomes ($n = 7$ for PBS and 6 for other groups). **f**, Tumour growth curves in bone marrow (BM) chimera mice. C57BL/6 WT mice reconstituted with WT BM (WT → WT, left) or *Alpk1*$^{-/-}$ BM (*Alpk1*$^{-/-}$→WT, middle) or *Alpk1*$^{-/-}$ mice reconstituted with WT BM (WT→*Alpk1*$^{-/-}$, right) were grafted with B16F10-OVA tumours and then treated with PBS ($n = 8$ for WT → KO and 6 for the other groups) or UDSP-Hep (50 µg per mouse; $n = 6$ for each group). **g**, scRNA-seq analysis of *Alpk1* and *Tifa* expression in intact B16F10-OVA tumours. Violin plots showing normalized *Alpk1* and *Tifa* expression across annotated cell clusters. **h**, Flow cytometry quantification of IFNγ^{hi} or GZMB^{hi} NK cells among CD45$^+$ cells in TILs of PBS or UDSP-Hep-treated MC38 tumours ($n = 8$ mice per group). **i**, Flow cytometry quantification of CD3$^+$ T cells and NK cells among CD45$^+$ cells in TILs of PBS or UDSP-Hep-treated B16F10-OVA tumours ($n = 8$ mice per group). **a**–**f**, **h**, **i**, Data are shown as mean ± s.e.m. Two-tailed unpaired Student's *t*-test or Welch's *t*-test (**h**, **i**), one-way ANOVA (**a**, **b**), and two-way ANOVA (**c**–**f**) were used for statistical comparisons. Data are representative of three (**c**–**f**) or two (**a**, **b**, **h**, **i**) independent experiments.

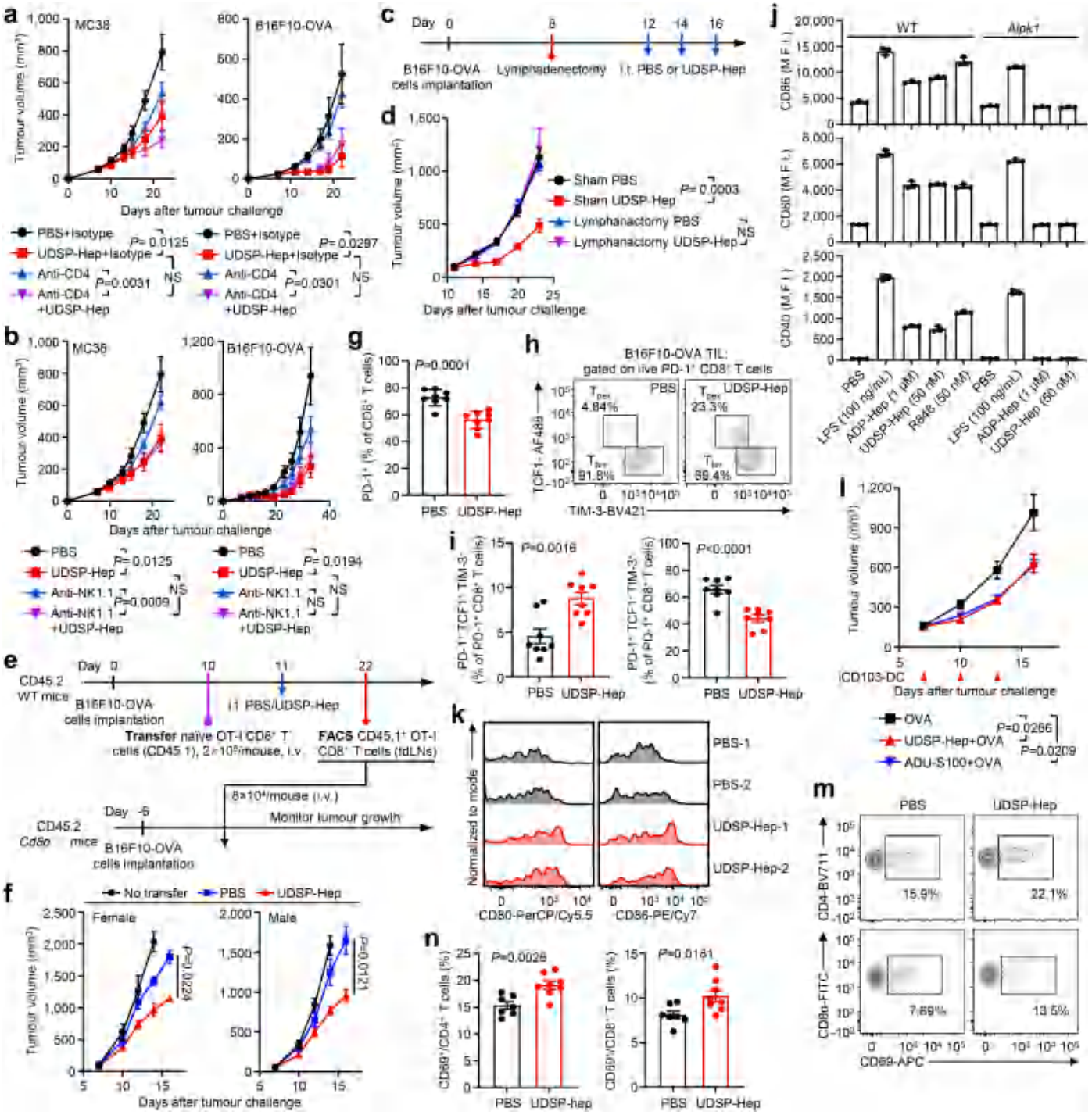

Extended Data Fig. 6 | See next page for caption.

Extended Data Fig. 6 | UDSP-Hep treatment activates DCs and T cells in the tdLN to control tumour growth. a, Growth curves of MC38 or B16F10-OVA tumours treated with PBS, UDSP-Hep, anti-CD4 depletion antibody, or UDSP-Hep combined with the depletion antibody ($n = 8$ for the PBS group of B16F10-OVA tumours and 9 for the other groups). **b**, Growth curves of MC38 or B16F10-OVA tumours treated with PBS, UDSP-Hep, anti-NK1.1 depletion antibody, or UDSP-Hep combined with the depletion antibody ($n = 9$ for MC38 tumour groups and 7 for B16F10-OVA tumour groups). The PBS and UDSP-Hep-alone groups in the left panel of **a** and **b** are the same as those in Fig. 4e. **c**, **d**, C57BL/6 mice bearing B16F10-OVA tumours were subjected to lymphadenectomy operation prior to PBS or UDSP-Hep treatment. **c**, Schematic diagram of the experiment. **d**, Tumour growth curves ($n = 5$). **e**, **f**, *CD8α*$^{-/-}$ mice receiving CD45.1$^+$ CD8$^+$ T cells adoptively transferred from tdLNs of B16F10-OVA-bearing donors treated with PBS or UDSP-Hep. **e**, Schematic diagram of the experiment. **f**, Tumour growth curves (female, $n = 4$ for PBS and 3 for other groups; male, $n = 4$ for UDSP-Hep and 5 for other groups). **g**, Flow cytometry quantification of PD-1$^+$ CD8$^+$ T cells among total CD8$^+$ T cells in PBS or UDSP-Hep-treated B16F10-OVA tumours (n = 8 mice per group). **h**, **i**, Analyses of CD8$^+$ T_{pex} and T_{tex} in the TILs of B16F10-OVA tumour-bearing mice treated with PBS or UDSP-Hep. **h**, Representative flow cytometry plots of anti-TCF1 and anti-TIM-3 staining. **i**, Quantification of the flow cytometry analyses (n = 8 mice per group). **j**, Quantification of the mean fluorescence intensity of anti-CD80, CD86, and CD40 staining of WT and *Alpk1*$^{-/-}$ iCD103-DCs treated with PBS, LPS, ADP-Hep, UDSP-Hep, or R848 (mean ± s.d., $n = 3$). **k**, Examination of cDC1s in tdLNs of PBS or UDSP-Hep-treated B16F10-OVA tumours. Shown are histograms of anti-CD80 and CD86 staining of the cDC1s. **l**, Purified iCD103-DCs were treated with 1 μg mL^{-1} OVA plus PBS, 100 nM UDSP-Hep, or 100 nM ADU-S100 for 8 h and then injected (1×10^5 per mouse) adjacent to the tdLN in B16F10-OVA-bearing mice on day 7, 10 and 13 after tumour challenge. Shown are tumour growth curves ($n = 9$ mice per group). **m**, **n**, Anti-CD69 staining of CD4$^+$ and CD8$^+$ T cells in tdLNs of PBS ($n = 7$) or UDSP-Hep ($n = 8$)-treated B16F10-OVA tumours. **m**, Representative flow cytometry plots. **n**, Quantification of CD69$^+$ populations among the T cells. **a**, **b**, **d**, **f**, **g**, **i**, **l**, **n**, Data are shown as mean ± s.e.m.; two-way ANOVA (**a**, **b**, **d**, **f**, **l**) and two-tailed unpaired Student's t-test (**g**, **i**, **n**), were used for statistical comparisons (NS, not significant). All data are representative of three independent experiments.

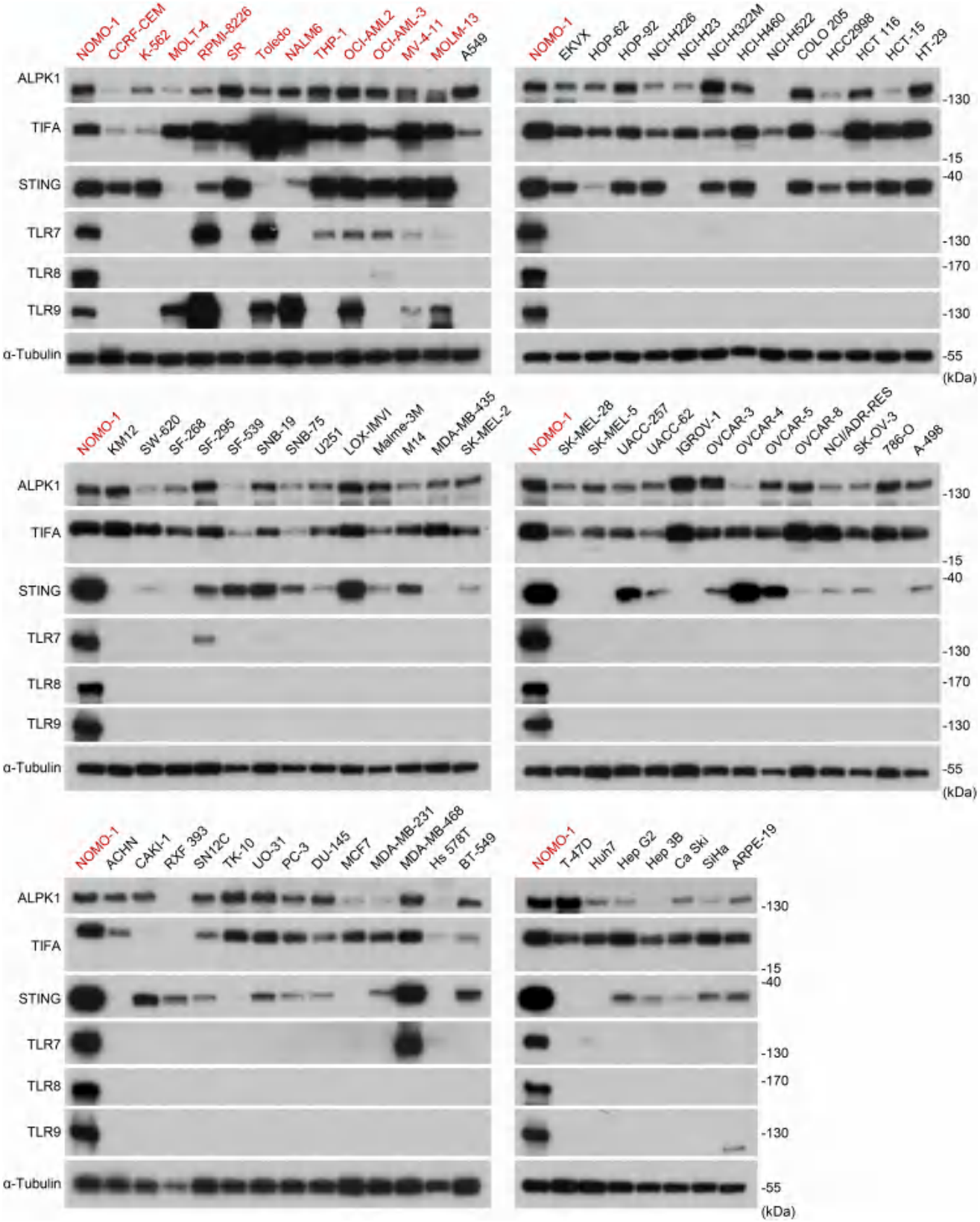

Extended Data Fig. 7 | Expression patterns of ALPK1, TIFA, STING, TLR7, TLR8, and TLR9 in NCI-60 plus 13 additionally selected cell lines. Cell lysates were blotted with indicated antibodies. Immune-relevant cells are marked in red. Data are representative of three independent experiments.

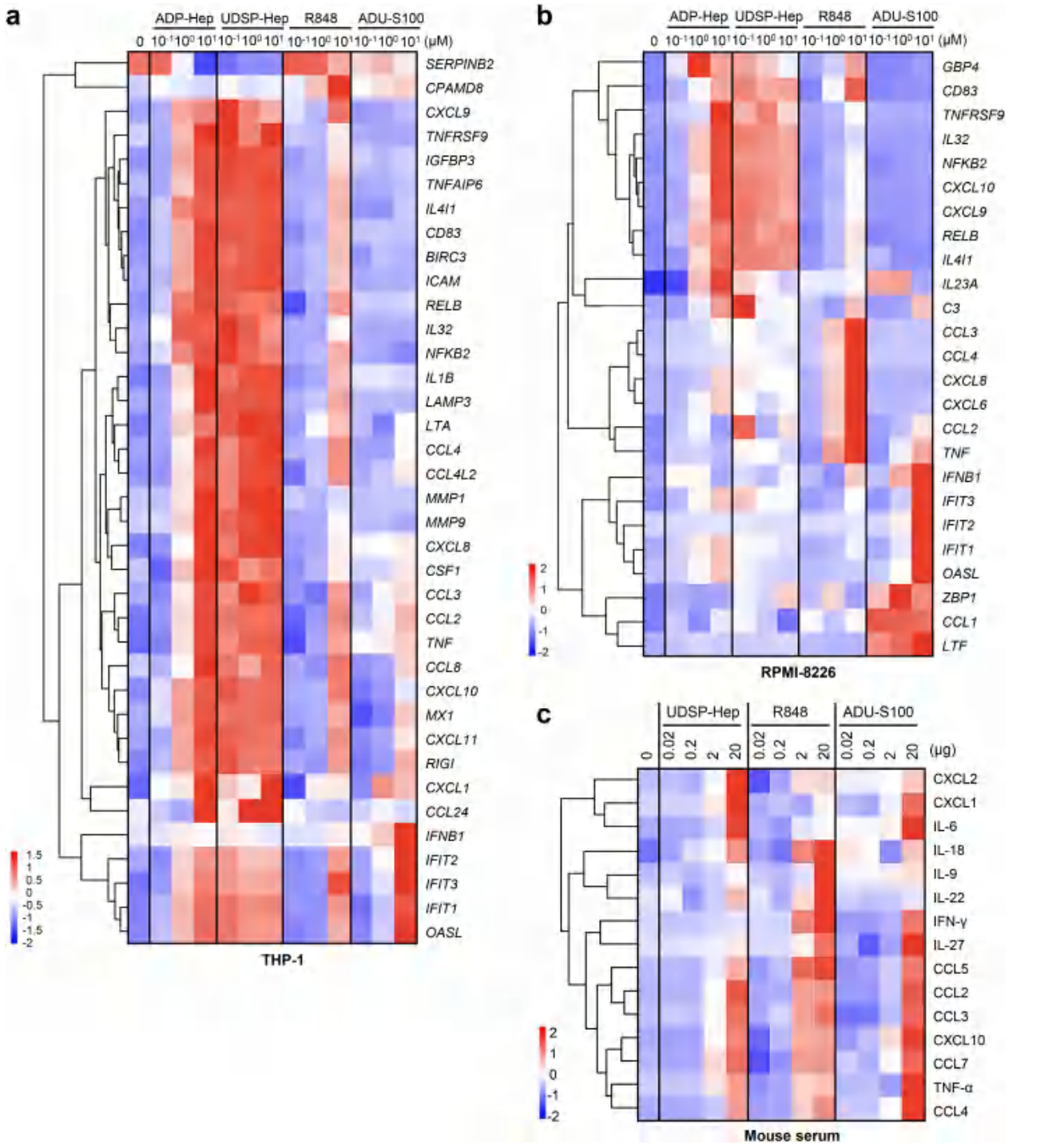

Extended Data Fig. 8 | Distinct transcriptional and cytokine signatures elicited by ALPK1, STING, and TLR agonists in immune-relevant cells and mice. a, **b**, Heatmap of gene expression in THP-1 monocytes (**a**) or RPMI-8226 B lymphocytes (**b**) treated with ALPK1 agonist (ADP-Hep or UDSP-Hep), TLR7/8 agonist (R848), or STING agonist (ADU-S100) at the indicated doses. Cells were treated for 4 h; mRNAs were isolated for RNA-seq analysis. **c**, Heatmap of cytokine concentrations in the sera of C57BL/6 WT mice injected (i.v.) with PBS, UDSP-Hep, R848, or ADU-S100 at the indicated doses (n = 5 for UDSP-Hep and R848 and 6 for ADU-S100). See Supplementary Fig. 8 for more comprehensive data. All data are representative of two independent experiments.

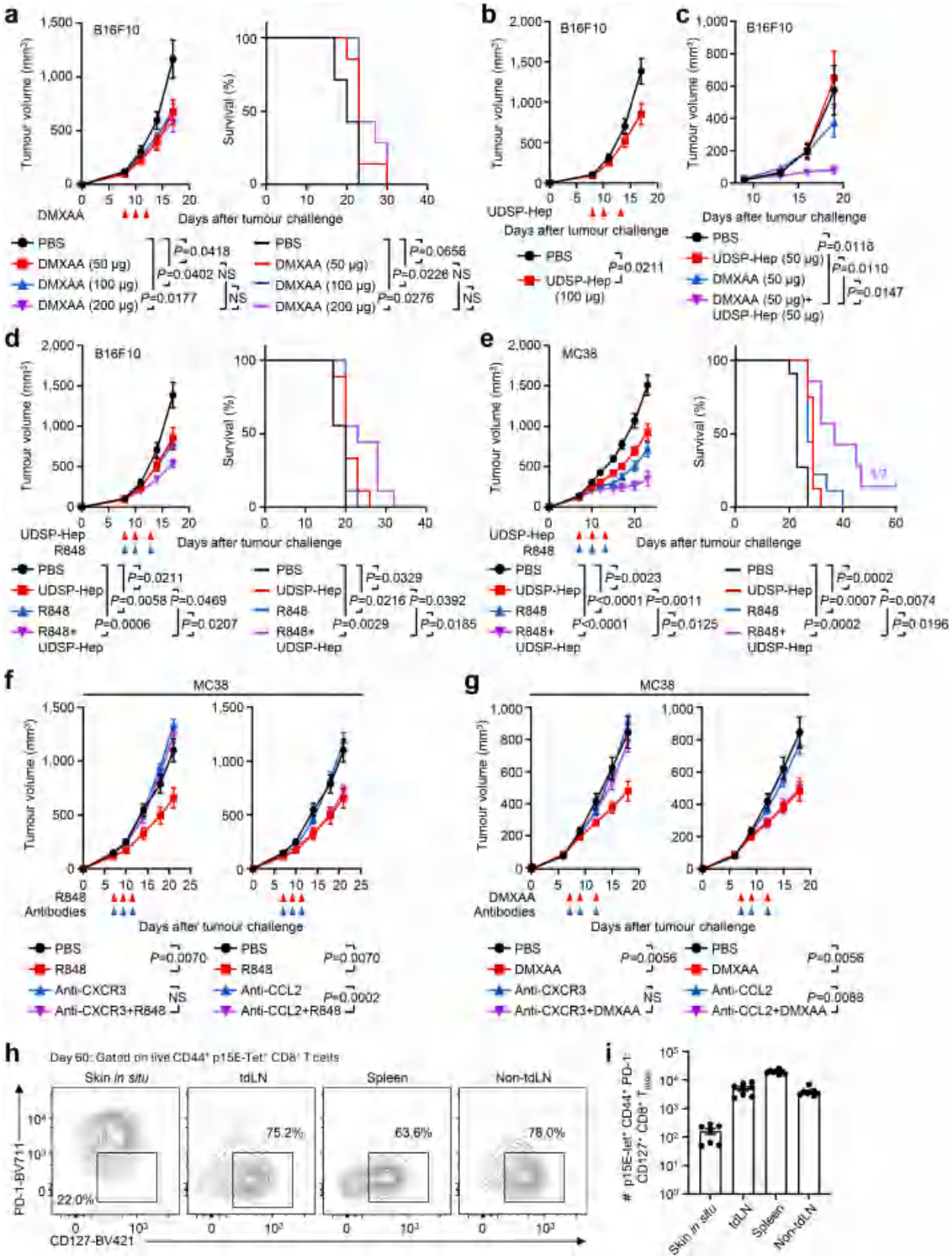

Extended Data Fig. 9 | See next page for caption.

Extended Data Fig. 9 | UDSP-Hep can act together with STING or TLR agonist to render enhanced antitumour activity. a, Growth curves (left) and mouse survival (right) of B16F10 tumours treated with PBS or DMXAA ($n = 7$ mice per group). **b**, Growth curves of B16F10 tumours treated with PBS or high-dose UDSP-Hep ($n = 9$ mice per group). This is the same experiment as the PBS and UDSP-Hep treatment groups in Extended Data Fig. 9d (left). **c**, Growth curves of B16F10 tumours treated with PBS, UDSP-Hep (50 μg per mouse), DMXAA (50 μg per mouse), or UDSP-Hep combined with DMXAA ($n = 9$ for PBS and 8 for other groups). **d**, **e**, Growth curves (left) and mouse survival (right) of B16F10 (**d**) and MC38 (**e**) tumours treated with PBS, UDSP-Hep (100 μg per mouse for B16F10; 50 μg per mouse for MC38), R848 (100 μg per mouse for B16F10; 50 μg per mouse for MC38), or UDSP-Hep combined with R848. **d**, $n = 9$ mice for each group. **e**, $n = 11$ for PBS, 8 for UDSP-Hep, 9 for R848, and 7 for UDSP-Hep combined with R848. **f**, **g**, Growth curves of MC38 tumours treated with R848 (50 μg per mouse, **f**) or DMXAA (50 μg per mouse, **g**) alone or in combination with CXCR3 blocking antibody (left) or CCL2 neutralizing antibody (right). **f**, $n = 12$ for PBS, 7 for R848 and anti-CXCR3 blocking antibody alone, 8 for CCL2 neutralizing antibody alone and R848 plus anti-CXCR3 blocking antibody, and 7 for R848 plus CCL2 neutralizing antibody. **g**, $n = 11$ for PBS, and 8 for all other groups. **h**, **i**, Measurements of the T_{tsm} population on day 60 in Hepa1-6 tumour-inoculated mice that already achieved complete tumour clearance by UDSP-Hep. Scheme of the experiments and the Day-23 data are in Fig. 5e–g. **h**, Representative flow cytometry plots gated on T_{tsm}. **i**, Quantification of the numbers of T_{tsm} at the inoculation site (Skin in situ), tdLNs, spleen, and non-tdLN ($n = 7$ for skin and 8 for other groups). **a**–**g**, **i**, Data are shown as mean ± s.e.m. Two-way ANOVA (**a**–**g**) and log-rank (Mantel–Cox) test (**a**, **d**, **e**) were used for statistical comparisons. All data are representative of three independent experiments.

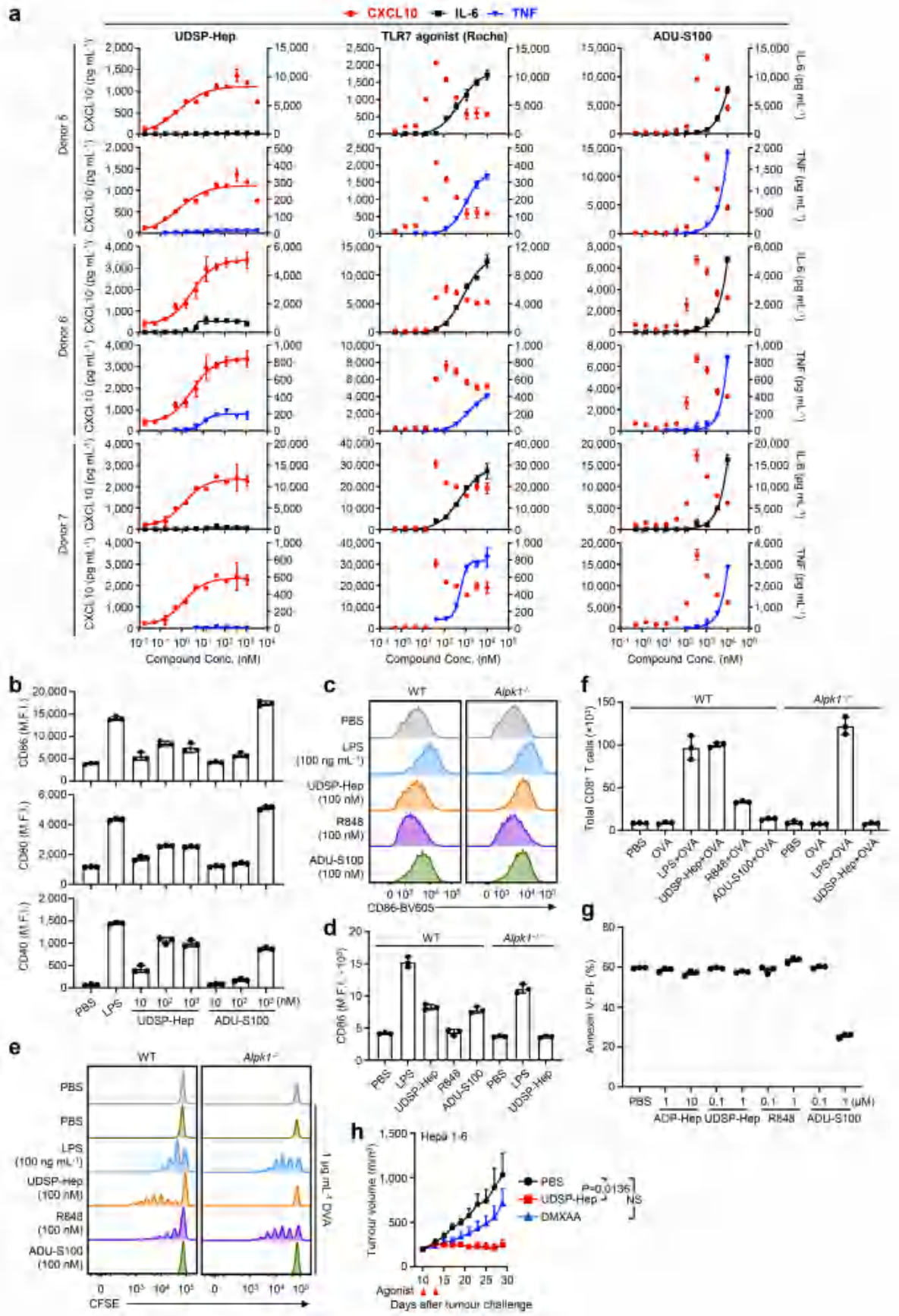

Extended Data Fig. 10 | See next page for caption.

Extended Data Fig. 10 | Comparisons of immune activation properties of ALPK1, STING, and TLR7/8 agonists. a, Induction of CXCL10, IL-6, and TNF by increasing doses of UDSP-Hep, the TLR7 agonist 41c-A from Roche, and ADU-S100 in human PBMCs (three donors). Shown are concentrations of the cytokines in the supernatants. **b**, Quantification ($n = 3$) of anti-CD86, CD80, and CD40 staining of purified iCD103-DCs treated with PBS, LPS, UDSP-Hep or ADU-S100. The histograms are shown in Fig. 5c. **c**, **d**, WT and *Alpk1*$^{-/-}$ BMDMs were treated with PBS, UDSP-Hep, R848, or ADU-S100. Shown are histograms (**c**) and quantification (**d**, $n = 3$) of anti-CD86 staining of the cells. **e**, **f**, OT-I $CD8^+$ T cells were co-cultured for 72 h with WT and *Alpk1*$^{-/-}$ BMDMs pre-stimulated with OVA alone or in combination with an indicated immune agonist. Shown are flow cytometry histograms (**e**) and quantification (**f**, $n = 3$) of total T-cell numbers. **g**, Viability of anti-CD3ε/CD28-activated mouse $CD3^+$ T cells after indicated treatments ($n = 3$). **h**, Growth curves of Hepa1-6 tumours treated with PBS, UDSP-Hep (50 μg per mouse), or DMXAA (50 μg per mouse) (mean ± s.e.m., $n = 8$ for PBS and 9 for other two groups). Two-way ANOVA was used for statistical comparisons. **a**, **b**, **d**, **f**, **g**, mean ± s.d. All data are representative of three independent experiments.